ForamEcoGENIE 2.0: Incorporating symbiosis and spine traits into a trait-based global planktic foraminifera model

Rui Ying[1], Fanny M. Monteiro[2], Jamie D. Wilson[1], Daniela N. Schmidt[1]

[1]School of Earth Sciences, University of Bristol, Bristol, BS8 1RJ, UK
[2]School of Geographical Sciences, University of Bristol, Bristol, BS8 1SS, UK

Correspondence to: Rui Ying (rui.ying@bristol.com)

Abstract. Planktic foraminifera are major marine calcifiers in the modern ocean regulating the marine inorganic carbon pump and generating marine fossil archives of past climate change. Some planktic foraminifera evolved spine and symbiosis, increasing functional trait diversity and expanding their ecological niches. Here we incorporate symbiosis and spine traits into the ForamEcoGENIE model, a trait-based model focusing on functional traits rather than individual species, to enable us to study the importance of foraminifera biodiversity in the palaeoceanographic environment. We calibrated the modelled new traits using Latin Hypercube Sampling. We identified the optimal model parameters from an ensemble of 1200 runs compared with observations from global core-tops, sediment traps, and plankton nets. The model successfully captures the global distribution and seasonal variation of the 4 major functional groups including dominance of the symbiont-obligate type in subtropical gyres and the symbiont-barren type in the productive subpolar oceans. The global annual mean biomass and foraminifer-derived carbon export rate is correctly predicted, with biomass from 0.001 to 0.010 mmol C m^{-3} and organic carbon export 0.002-0.031 mmol C m^{-2} d^{-1}. The seasonal peak time of biomass and organic carbon export are also generally captured. although the amplitude is not able to be reproduced in productive area. Both the sparseness of observations and the model's limitation in upwelling regions likely contributes to the discrepancy. Our model overcomes the lack of biodiversity in previous version and offers the potential to explore foraminifera ecology dynamics and its impact on biogeochemistry in modern, future and paleogeographic environments.

Deleted: ed

Deleted: best

Deleted: run

Deleted:

Deleted: for spinose foraminifera, but the model overestimates the global mean biomass of each group by 8 times and global export rate of non-spinose foraminifera by 4 times

Deleted: The calcite export is mostly derived from the symbiont-barren non-spinose group (39%) and the symbiont-obligate spinose group (13%).

Deleted: observational bias

Deleted: linking biomass to export production

Deleted: Our model approximates a 3.05 g m^{-2} yr^{-1} global mean foraminifer-derived calcite flux and 1.1 Gt yr^{-1} total calcite export, account for 19% of the global pelagic marine calcite budget within the lower range of modern calcite estimates. The calcite export is mostly derived from the symbiont-barren non-spinose group (39%) and the symbiont-obligate spinose group (13%).

1 Introduction

Planktic foraminifera are marine calcifying zooplankton that have populated the surface ocean since the mid-Jurassic (~175 Ma). They produce calcite shells (or "tests"), preserved in vast amounts in sediments, that provide proxy archives (e.g., ^{13}C, ^{18}O, Mg/Ca) to reconstruct past climate conditions (Tierney et al., 2020), ocean carbonate chemistry (Hönisch et al., 2012) and study biotic response to environmental change (Todd et al., 2020). In the modern oceans, foraminifera contribute 23-56% of the total open-ocean $CaCO_3$ export (Schiebel, 2002) alongside the other major calcifiers, coccolithophores (Daniels et al., 2018) and pteropods (Buitenhuis et al., 2019). However, understanding the impacts of environmental change on foraminifers and their role in the carbon cycle is challenged by their low standing stocks in the surface ocean, a (semi)lunar reproductive cycle driving abundances and difficulties in culturing to ground truth physiology (Schiebel and Hemleben, 2017). Modelling planktic foraminifera and their ecology, therefore, plays a critical role in increasing and testing our understanding of their biological and ecological influence on the marine inorganic carbon cycle and their role as a paleo-proxy carrier

The recent decades have seen significant developments of global foraminifera models due to the increasing data compilations of foraminifer flux and community structure (Siccha and Kucera, 2017; Buitenhuis et al., 2013; Sunagawa et al., 2020). But they are either empirical based or limited to the extant species. For example, Waterson et al., (2017) built a Maxent species distribution models based on sediment core data to study the niche variability from Last Glacial Maximum (LGM) to Holocene. Žarić et al. (2006) constructed the statistical model that correlated hydrographical factors and sediment trap abundance of 18 main species. Such correlative models have limitation on predicting future projection because the assumption of constant correlation with environmental factors can be violated (Buckley et al., 2010). In addition, niche models also are ignorant in biological interactions which have an important role in shaping species distribution. On the other hand, although Fraile et al. (2008) and Lombard et al. (2011) have built ecophysiology-based mechanistic models PLAFOM and FORAMCLIM which successfully reconstructed planktic foraminifer's geographical distribution, seasonal and vertical population dynamics (Kretschmer et al., 2018) and held the abilities to simulate in different climatology like the LGM (Fraile et al., 2009) or projected high-emission future (Roy et al., 2015), these two models are species-based and therefore cannot be applied in the deeper times older than the Miocene with many extinct species and cryptic taxa with novel ecologies (Renaud and Schmidt, 2003). Thus, to fill the model gap of not able to leverage the abundant foraminifer fossil information, a mechanistic model but not limited to any species is needed

Trait-based plankton models as an alternative to species-based models come into vision under such circumstance. This approach which focuses on organismal traits including morphological and physiological properties instead of taxonomic identities provides a mechanistic way to mimic the complex real ocean ecology by defining traits' functional benefits and costs (i.e., trade-offs) (Zakharova et al., 2019; Kiørboe et al., 2018). Models adopting trait-based framework have successfully resembled the diverse marine community such as cyanobacteria (Follows et al., 2007) and diazotroph (Monteiro et al., 2010)

Deleted: ¶

Deleted: (

Deleted:

Deleted: first global-scale prediction on foraminifer flux using a

Deleted: technique

Deleted:

Deleted: an ecophysiology based dynamic

Deleted: based on CESM (Hurrell et al., 2013) and PISCES (Aumont et al., 2015), respectively. These two models

Deleted: production

Deleted: in Last Glacial Maximum (LGM) (Fraile et al., 2009), vertical distribution dynamics

Deleted: potential diversity change in response to

Deleted: projected

Deleted: scenarios

Deleted: .

Deleted: However

Deleted: , the species-based feature of these models causes limitations for applications.

Deleted: For example, parameterisation limits the inclusion of additional species, which are less well understood ecologically. Moreover, while these models are applied to LGM and future oceans, the application to deeper time is severely limited by the existence of extinct species and cryptic taxa with novel ecologies (Renaud and Schmidt, 2003) and non-analogue situations, i.e., time intervals older than the Miocene with many none extant species, cannot be assessed with confidence.¶

Deleted: T

Deleted: of plankton

Deleted: ecology can overcome the challenges of

Deleted: .

Deleted: to reduce model complexity

Deleted: , capture ecological interaction

Deleted: and identify drivers of community assembly under global changes (Enquist et al., 2015).

Deleted: , usually by defining physiological characteristics and relevant trade-offs (e.g., size-class of plankton)

This strategy is also well suitable for planktic foraminifer because functional traits like body size (Schmidt et al., 2004), size normalised weight (Todd et al., 2020), and symbiosis (Spero and Parker, 1985) have been widely measured and studied. And such functional traits have been consistently evolved in foraminifera across Cenozoic (Ezard et al., 2011). Next we provide the brief introduction for spine and symbiosis traits that determine species-level ecological and functional distinguishment and also compose of the focus of this model study.

Nearly 19 out of 50 modern foraminifer species bear eukaryotic algae such as dinoflagellates, chrysophytes and haptophyte as symbionts (Takagi et al., 2019). Compared to non-symbiont species (termed as "symbiont-barren") that live in temperate and polar oceans, symbiotic species dwell in the tropical to subtropical regions (see biogeography in Figure 3) where their symbionts are facilitated to photosynthesize and providing an extra energy pathway to foraminifera in the nutrient-deficient environment (LeKieffre et al., 2018; Ortiz et al., 1995; Uhle et al., 1999). The symbiotic group can be further partitioned because some foraminifers that cannot live without their symbionts (termed as "symbiont-obligate") (Bé et al., 1982) while others are flexible (termed as "symbiont-facultative"). As the symbionts affecting latitudinal distribution of foraminifer, the calcareous spine trait shows importance in shaping feeding behaviour Non-spinose foraminifera rely on rhizopodia to capture prey, but spinose foraminifer with spines extruding from the test have larger effective reach range and stronger ability to active prey, which leads to more prey types and sizes like large copepods (Anderson et al., 1979). Laboratory observations show the spinose foraminifera's carnivory preference with the zooplankton/phytoplankton prey protein ratio from 117:1 to 278:1 (Schiebel and Hemleben, 2017, Section 4.1). And the effective encounter rate of a spinose genus can be three orders of magnitude higher than non-spinose foraminifer (Gaskell et al., 2019). Furthermore, roughly half of modern species are spinose, therefore this trait is non-negligible. Based on the presence of these two functional traits, the foraminifera can be divided into four functional types: (1) symbiont-barren non-spinose; (2) symbiont-barren spinose; (3) symbiont-facultative non-spinose; (4) and symbiont-obligate spinose (Table 1).

Recently, Grigoratou et al., (2019) developed the first mechanistic and trait-based 0D model for symbiont-barren non-spinose foraminifer and coupled it to cGENIE (ForamEcoGENIE 1 hereafter, Grigoratou et al., 2021a), an 3D Earth System Model of intermediate complexity allowing for fast computational time and widely applied to past climates: Palaeocene–Eocene Thermal Maximum (Ridgwell and Schmidt, 2010), Last Glacial Maximum (Rae et al., 2020) and Cretaceous-Paleogene boundary (Henehan et al., 2019). Such computational efficiency and abundant applications make ForamEcoGENIE easily applicable to a wide range of geological periods with direct links with seawater carbon chemistry and isotope tracers. In this study, we extend ForamEcoGENIE to resolve 3 more critical functional groups of planktic foraminifera by adding the traits of symbiosis and spines (tested in Grigoratou et al., 2021b). Thereby, we build a model that can explore foraminifer diversity in past climates (Ezard et al., 2011). We compare the model with three global observational data compilations (core-top, plankton net tow and sediment traps) and test its ability to produce surface biomass, organic carbon and calcite flux, and relative abundance distribution.

Deleted: Undoubtedly, this strategy provides a simple but mechanistic way to mimic the complex real ocean ecology (Kiørboe et al., 2018).

Deleted: ¶
Understanding of foraminifer traits and their functions is crucial for developing a trait-based model. The foremost trait of foraminifer is calcification, with foraminifera building a shell by adding calcite chambers during their development (Caromel et al., 2015). In addition, 19 out of ~50

Deleted: Spines and symbiosis are crucial functional traits of planktic foraminifers and dividing the group in their phylogeny study (Morard et al., 2018). S

Deleted: assimilate

Deleted: nutrients, which can be translocated to the host,

Deleted: to the foraminifer

Deleted: Core-top data (Siccha and Kucera, 2017) show that species with symbionts are mainly found in the low latitudes and open oceans, while non-symbiotic foraminifers dominate the temperate to polar regions (Figure 1). Furthermore, symbiont-obligate

Deleted: prefer the low latitude to the symbiont-facultative group which can flexibly bear symbionts and have a wider geography (Figure 1). Another important trait is

Deleted: s

Deleted: extruding from the test, present in roughly half of modern species

Deleted: .

Formatted: English (US)

Deleted: (Anderson et al., 1979) These spinose species are mostly symbiotic (except symbiont-barren *Globigerina bulloides* and *Hastigerina pelagica)* and show a preference for omnivorous feeding (Schiebel and Hemleben, 2017). Therefore, traits affect biogeography and trophic activities and lay the foundation of building a trait-based model.¶

Deleted: trait-based

Deleted:

Deleted: ecogroups

Deleted: flux rate

2 cGENIE ocean and atmosphere physics

ForamEcoGENIE uses cGENIE (carbon-centric Grid-ENabled Integrated Earth system model), a modular Earth system model of intermediate complexity (EMIC) as the physical ocean simulation framework. The fast climate and ocean physics of cGENIE are based on a coarse-resolution 3D frictional geostrophic ocean model coupled to a 2D energy-moisture-balance atmosphere model and a dynamic-thermodynamic sea-ice model (Edwards and Marsh, 2005; Marsh et al., 2011). The ocean has a 36x36 equal-area horizontal grid (uniform in longitude and sine-uniform in latitude) with 16 logarithmically spaced vertical levels as defined in Cao et al., (2009). The physical model is coupled with a model of ocean biogeochemical cycles (Ridgwell et al., 2007; van de Velde et al., 2021), sea-floor sedimentary processes (Ridgwell and Hargreaves, 2007) and marine ecosystem processes (Ward et al., 2018). The plankton ecosystem is resolved in the surface layer (0-80.8 m) to mimic light limitation. The model presented in this study is configured with a seasonally forced pre-industrial climate state and a fixed atmospheric CO_2 concentration restored to 278 ppm.

3 Size-based plankton ecosystem framework EcoGENIE

3.1 Biogeochemical tracers

The model has three biogeochemical tracers (noted in i_r): carbon, phosphorus, iron. The plankton biomass has same tracers (i.e., C, P, Fe) with notation i_b for each plankton group j. And phytoplankton or symbiotic foraminifera have an extra state variable for chlorophyll (Chl hereafter). These elements are marked in different colors in Figure 1.

3.2 Plankton cell size and quota

In EcoGENIE, individual body size determines key physiological processes, including nutrient uptake, photosynthesis, grazing gain and predation through allometric scaling (West et al., 1997), because of its role as a master trait among pelagic organisms (Andersen et al., 2016). The modelled size-dependent parameters (except for photosynthesis) follow a generic power law: $P = aV^b$ with P the size-based parameter, V the spheric biovolume, and a, and b the allometric intercept and exponent.

A fundamental size-based concept of EcoGENIE is the plankton cell quota for various elements. The carbon quota content (Q_C) follows a power law determining by plankton size (biovolume, V), scaling coefficient a and exponent b (Equation 1). And then the variable stoichiometry ($\mathrm{Q}_{\mathrm{i}_\mathrm{b}}$, Eqn. 2) is achieved by the ratio of assimilated nutrients biomass (B_{i_b}, i_b stands for P, Fe, or chlorophyll) to carbon biomass (B_C) (Droop, 1968; Flynn, 2008). This stoichiometry will limit nutrient uptake rate ($Q_{i_b}^{\mathrm{stat}}$, Eqn. 3) as per Geider et al., (1998), with higher value close to its maximum ($\mathrm{Q}_{\mathrm{i}_b}^{\mathrm{max}}$), lower the nutrient uptake or chlorophyll synthesis rate . The nutrient quota range ($\mathrm{Q}_{\mathrm{i_b}}^{\mathrm{min}}$, $\mathrm{Q}_{\mathrm{i}_b}^{\mathrm{max}}$) is proportional to the carbon quota (Q_C).

$$Q_C = \mathrm{a}\mathrm{V}^b \tag{1}$$

Deleted: ¶

(a) symbiont-barren non-spinose: mean= 25.61%

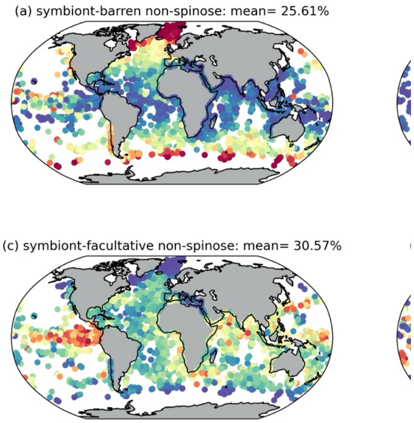

(c) symbiont-facultative non-spinose: mean= 30.57%

Formatted: Justified

Deleted: Figure 1: Relative proportion in shell abundance of planktic foraminifer functional groups. Data source: ForCenS ... [1]

Deleted: 2

Deleted: Model description¶
2.1 Ocean and atmosphere physics¶ ... [2]

Formatted: Normal

Formatted: Font: 10.5 pt, Bold

Formatted: Font: 10.5 pt, Bold

Formatted: Font: 10.5 pt, Bold

Formatted: English (UK)

Formatted: Normal

Formatted: Font: Italic, English (UK)

Formatted: Font: Italic, English (UK), Subscript

Formatted: Font: Not Italic, English (UK), Not Superscript/ Subscript

Formatted: English (UK), Not Superscript/ Subscript

Formatted: Font: Italic, English (UK), Not Superscript/ Subscript

Formatted: Font: Not Italic, English (UK)

Formatted: English (UK)

Formatted: Font: Times New Roman

Formatted: Font: Bold

Formatted: Font: Bold

$$Q_{i_b} = \frac{B_{i_b}}{B_C}, \qquad i_b = P, Fe, Chl \qquad (2)$$

$$Q_{i_b}^{\mathrm{stat}} = \left(\frac{\mathrm{Q}_{\mathrm{i}_b}^{\max} - \mathrm{Q}_{\mathrm{i_b}}}{\mathrm{Q}_{\mathrm{i}_b}^{\max} - \mathrm{Q}_{\mathrm{i_b}}^{\min}}\right)^{0.1} \qquad (3)$$

3.3 Plankton biomass dynamics

The biomass of any plankton group (*j*) and element (*iь*), $\mathrm{B_{j,i_b}}$, varies due to a combination of potential physiological processes that are determined by the type of organism: nutrient uptake, grazing gains, grazing losses, mortality, and respiration losses (Eqn. 5). Foraminifer-related specific processes will be introduced in following sections. We refer readers to Ward et al. (2018) for more detailed description of EcoGENIE model, although some of them might overlap.

$$\frac{\partial \mathrm{B_{j,i_b}}}{\partial \mathrm{t}} = \underbrace{\mu_{\mathrm{j,i_b}} \cdot \mathrm{B_{j,C}}}_{nutrient\ uptake} + \underbrace{\mathrm{B_{j,C}} \cdot \lambda_{\mathrm{i_b}} \sum_{\mathrm{j_{prey}}=1}^{\mathrm{J}} \mathrm{G_{j,j_{prey},i_b}}}_{grazing\ gains}$$

$$- \underbrace{\mathrm{B_{j_{pred},C}} \cdot \sum_{\mathrm{j_{pred}}=1}^{\mathrm{J}} \mathrm{G_{j_{pred},j,i_b}}}_{grazing\ losses} - \underbrace{\mathrm{m_j} \cdot \mathrm{B_{j,i_b}}}_{mortality\ loss} - \underbrace{\mathrm{r_{j,C}} \cdot \mathrm{B_{j,i_b}}}_{respiration\ loss} \qquad (4)$$

3.4 Inorganic nutrient dynamics

The inorganic resource state variables (R_{i_r}) varies with nutrient uptake (V_{j,i_r}) and dissolved inorganic carbon (DIC) with the living organisms' respiration ($r_{j,C}$).

$$\frac{\partial R_{i_r}}{\partial t} = \begin{cases} \sum_{j=1}^{J} -\mu_{j,i_r} \cdot B_{j,C}, & i_r = Fe, P \\ \sum_{j=1}^{J} -\mu_{j,i_r} \cdot B_{j,C} + \sum_{j=1}^{J} r_{j,C}, & i_r = C \end{cases} \qquad (5)$$

Additional sources and sinks of nutrients such as remineralisation of organic matter and air-sea gas exchange are computed in the biogeochemical module BIOGEM (Ridgwell et al., 2007).

3.4 Organic matter dynamics

Organic carbon flux (F) comes from and predators' messy feeding and the mortality loss from all plankton groups (Eqn. 6).

$$F = \sum_{j_{\mathrm{prey}}=1, j_{\mathrm{pred}}=1}^{J} \left(1 - \beta_{j_{\mathrm{prey}}}\right)\left(1 - \lambda_{j_{\mathrm{pred}}}\right) G_{j_{\mathrm{pred}}, j_{\mathrm{prey}}} B_{j_{\mathrm{pred}}} + \sum_{j_{\mathrm{plankton}}=1}^{J} \left(1 - \beta_{j_{\mathrm{plankton}}}\right) m_{j_{\mathrm{plankton}}} B_{j_{\mathrm{plankton}}} \qquad (6)$$

Deleted: ¶
We employ the trait-based marine plankton ecosystem model EcoGENIE (Ward et al., 2018) to simulate foraminifera's physiological processes and ecological interactions with other plankton. In this section, we summarise the core concepts specific to foraminifera modelling and refer the readers to Ward et al. (2018) for the full description of the model.¶
In EcoGENIE, individual body size determines key physiological processes, including nutrient uptake, photosynthesis, grazing gain and predation through allometric scaling (West et al., 1997), because of its role as a master trait among pelagic organisms (Andersen et al., 2016). The modelled size-dependent parameters (except for photosynthesis) follow a generic power law: $P = aV^b$ with P the size-based parameter, V the spheric biovolume, and a, and b the allometric intercept and exponent.¶

Deleted: A fundamental size-based concept is the plankton cell quota. The plankton size (biovolume, *V*) determines the carbon quota content (Q_C) following a power law (with scaling coefficient *a*nd exponent *b*, Equation 1). ($\mathrm{Q_{i_b}}$, Eqn. 2) The ratio of other assimilated nutrients (B_{i_b}, *iь* stands for the *i*th population nutrient biomass: P, Fe, or chlorophyll) to carbon biomass (B_C) represents the plankton group's physiological status with dynamic stoichiometry ($\mathrm{Q_{i_b}}$, Eqn. 2) (Droop, 1968; Flynn, 2008). ($\mathrm{Q}_{\mathrm{i}_b}^{\max}$, Eqn. 3)Based on this cell quota status, the limitation term for each nutrient ($Q_{i_b}^{\mathrm{stat}}$) is formulated as per Geider et al., (1998), where nutrient uptake rate gradually slows down when the internal inorganic nutrient quota is close to its maximum value ($\mathrm{Q}_{\mathrm{i}_b}^{\max}$, Eqn. 3). The nutrient quota range ($\mathrm{Q}_{\mathrm{i_b}}^{\min}$, $\mathrm{Q}_{\mathrm{i}_b}^{\max}$) is proportional to the carbon quota (Q_C).¶

$Q_{i_b} =$

$Q_{i_b}^{\mathrm{sta}}$

Metabolic processes in EcoGENIE are temperature dependent, as in the universal metabolic theory (Brown et al., 2004). Ectothermic plankton's body temperature is determined by the ambient seawater environment (*T*). Temperature regulation γ_T acts on metabolic processes including respiration, nutrient uptake, and predation and is modelled through an Arrhenius-like function (Eqn. 4), where the parameter *A* determines temperature sensitivity and reference temperature (T_{ref}) is the temperature allowing $\gamma_T = 1$.¶

Formatted: Font: Bold

Formatted: Font: Bold

Deleted: DIC

$\beta_{j_{\text{prey}}}$ is the fraction of dissolved organic carbon (DOC) subject to advection by ocean circulation, and the remaining fraction is the particulate organic carbon (POC) subject to redistribution through the water column by sinking. Parameter β is defined by a size-based sigmoid function depending on maximum and minimum DOC fraction (β_{max}, β_{min}), and the size β_s at which DOC/POC ratio equals 1 (Ward and Follows, 2016). The proportion of DOC therefore decreases with plankton cell size.

$$\beta = \beta_{max} - \frac{\beta_{max} - \beta_{min}}{1 + \beta_s/ESD} \tag{7}$$

Messy feeding behaviour is modelled as unassimilated carbon fraction $(1 - \lambda_{j_{\text{pred}}})$ of prey which is limited by the size-independent maximum efficiency coefficient (λ_m) and the nutrient limitation (Fe or P).

$$\lambda = \lambda_m \cdot min[Q_P^{\text{stat}}, Q_{Fe}^{\text{stat}}] \tag{8}$$

3.5 Plankton community structure

The EcoGENIE plankton ecosystem model can be defined in flexible size structure. In both ForamECOGENIE 1 and 2, we resolve eight size classes of phytoplankton, seven size classes of zooplankton and one size class for each of the four foraminifer groups. Phytoplankton and zooplankton size classes include 0.6, 1.9, 6.0, 19.0, 60.0, 190.0, 600.0 and 1900.0 µm. The foraminifer cell size is set to an Equivalent Sphere Diameter (ESD) of 190 µm, which is typical for an adult foraminifer (Grigoratou et al., 2019).

4 ForamEcoGENIE 1 description

ForamEcoGENIE 1 accounted for the feeding behaviour and calcification of foraminifera (Grigoratou et al., 2019, 2021a). It implemented a predator-prey interaction ($G_{j_{\text{pred}},j_{\text{prey}}}$, Eqn. 9) using a Holling type II model (Holling, 1965), where the overall grazing rate depends on the total available prey ($F_{j_{\text{pred}}}$), the maximum grazing rate of predators (G_{pred}^m) and the half-saturation concentration of available food ($k_{j_{\text{prey}}}$), and is regulated by temperature limitation (γ_T), a prey-switching term (Φ), and a prey refuge protection $(1 - e^{\Lambda F_{j_{\text{pred}}}})$. The calcification trait was included by reducing foraminifera palatability (P_p which influences $F_{j_{\text{pred}}}$, Eqn. 10) and mortality rate (m_j, Eqn. 5) to account for higher protection against predators and infections to the expense of a lower G_{foram}^m (Eqn. 9). To avoid repeating, we also introduce the ForamEcoGENIE 2 parameters (spine effect τ and a mixotrophy limitation λ_h) here. Readers may assume they equal one, i.e., no functioning in ForamEcoGENIE 1.

$$G_{j_{\text{pred}},j_{\text{prey}}} = \underbrace{\gamma_T \cdot \lambda_h}_{\text{limitations}} \cdot \underbrace{\frac{G_{pred}^m F_{j_{\text{pred}}}}{\tau k_{j_{\text{prey}}} + F_{j_{\text{pred}}}}}_{\text{overall grazing rate}} \cdot \underbrace{\Phi_{j_{\text{pred}},j_{\text{prey}}}}_{\text{Switching}} \cdot \underbrace{\left(1 - e^{\Lambda F_{j_{\text{pred}}}}\right)}_{\text{prey refuge}} \tag{9}$$

$$F_{j_{\text{pred}}} = P_p \cdot B_{j_{\text{prey}}} \cdot \exp\left[-ln\left(\frac{\mu_{j_{\text{pred}},j_{\text{prey}}}}{\mu_{\text{opt}}}\right)^2 / 2\sigma_{j_{\text{pred}}}^2\right] \tag{10}$$

Deleted: ¶
2.3 ForamEcoGENIE

Deleted: .0

Deleted: .0

Deleted: two foraminifera traits, including

Deleted: 7

Deleted: 8

Deleted: 7

Formatted: Font: (Default) SimSun, (Asian) SimSun

Deleted: ϵ

Deleted: 7

In the model, the predators select their preys (Eqn. 10) based on the predator-prey size ratio $\mu_{j_{\mathrm{pred}},j_{\mathrm{prey}}}$ relative to the optimal value μ_{opt}, predators' food range $\sigma^2_{j_{\mathrm{pred}}}$, and the calcification protection P_p. Foraminifera in both ForamEcoGENIE 1 and 2 were set as herbivores.

The grazing process like other metabolisms in EcoGENIE are temperature dependent, as in the universal metabolic theory (Brown et al., 2004). Ectothermic plankton's body temperature is determined by the ambient seawater environment (T). Temperature regulation γ_T acts on metabolic processes including respiration, nutrient uptake, and predation and is modelled through an Arrhenius-like function (Eqn. 12), where the parameter A determines temperature sensitivity and reference temperature (T_{ref}) is the temperature allowing $\gamma_T = 1$.

$$\gamma_T = e^{A(T-T_{\mathrm{ref}})} \qquad (11)$$

The prey-switching term ($\Phi_{j_{\mathrm{pred}},j_{\mathrm{prey}}}$) simulates the feeding habitat of zooplankton (Eqn. 9). The exponential s defines the active level of zooplankton predators, which capture abundant prey with higher priority when s increases. Foraminifera both in ForamEcoGENIE 1 and 2 are assumed to be ambush passive predators with s=1.

$$\Phi_{j_{\mathrm{pred}},j_{\mathrm{prey}}} = \frac{\left(F_{j_{\mathrm{pred}}}\right)^s}{\sum_{j_{\mathrm{prey}}=1}^{J}\left(F_{j_{\mathrm{pred}}}\right)^s} \qquad (12)$$

Finally, to further approach the reality, the refuge term $(1 - e^{\Lambda F_{j_{\mathrm{pred}}}})$ in the Eqn. (9) is added to decrease grazing rate when prey availability lowers with the protection strength of Λ.

5 ForamEcoGENIE 2: improved calcification and more functional groups

In ForamEcoGENIE 2, we expand the first version by adding symbiosis and spine traits to the foraminifera group to distinguish four functional groups of planktic foraminifera (Table 1, Figure 1). We also implement a new calcification trade-off relating calcification energetic cost to the respiration term.

Table 1. The four modelled functional groups of planktic foraminifera and their species representative in ForamEcoGENIE 2.0.

Spine trait	Symbiosis trait	Species example	Species number*	Model implementation
Spinose	Symbiont-obligate	*Globigerinoides ruber*	17	This study
Spinose	Symbiont-barren	*Globigerina bulloides*	*2*	This study
Non-spinose	Symbiont-facultative	*Neogloboquadrina dutertrei*	*5*	This study

Deleted: 8

Deleted: The f

Deleted: .0

Deleted: Additional foraminifera traits defined by a spine effect (ϵ) and a mixotrophy cost (λ_h) are introduced in ForamEcoGENIE 2.0 (see section 2.4)

Formatted: Font: (Asian) +Body Asian (DengXian)

Deleted: 7

Deleted: All f

Deleted:

Deleted: 7

Deleted: 2.4

Deleted: .0

Deleted:

Deleted: Here

Deleted: ForamEcoGENIE 1

Deleted: .0

Formatted: English (US)

Non-spinose	Symbiont-barren	*Neogloboquadrina pachyderma*	23	extended from ForamEcoGENIE 1.0

* Count from Schiebel and Hemleben, (2017)

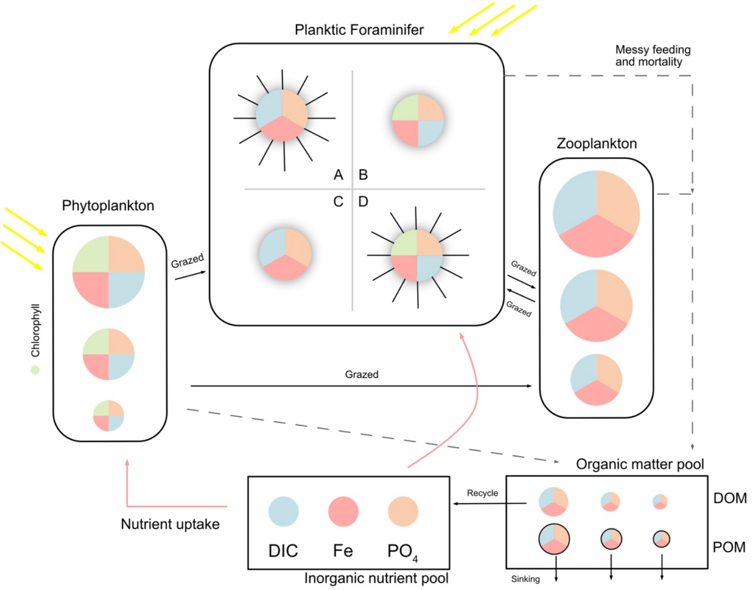

Figure 1. Schematic diagram of ForamEcoGENIE structure, showing the biogeochemical tracers (C, Fe, PO_4) in different colors and plankton populations with various size classes. Physiological processes here include nutrient uptake (red arrows), organic matter production caused by messy feeding and mortality (dashed arrows), and zooplankton grazing (black arrows). A. symbiont-barren spinose group; B. Symbiont-facultative non-spinose group; C. symbiont-barren non-spinose group. D. symbiont-obligate spinose group. DIC: dissolved inorganic carbon.

5.1 Calcification trait trade-offs

5.1.1 Benefit: Mortality protection

Deleted: 2.4

Deleted: Respiration cost

Deleted: ¶
We modified the metabolic cost of calcification defined in Grigoratou et al. (2019, 2021a) by replacing the original reduced maximum growth rate (or specifically maximum grazing rate) with a temperature-dependent respiration loss term. We choose this new loss term over a reduced growth rate because (1) extra respiration is a more biologically realistic cost and (2) a temperature-dependent term helps reduce the low-latitude biomass as observed.¶
Metabolic cost¶
The respiration r_j present in Eqn. 5 scales with carbon biomass and is multiplied by constant r_b and temperature limitation (Eqn. 10). We assumed that the lost carbon from respiration is instantly recycled back to DIC pool.¶

Deleted: a

Deleted: .

Formatted: Font: Not Italic

The mortality loss term in the generic zooplankton scales with a basal rate constant m_b (Eqn. 5). Like in Grigoratou et al. (2019, 2021a), m_b for foraminifera is downscaled by a protection term P_m where a lower value of m_j indicates a higher protection from the foraminifera test against viral and bacterial infections.

$$m_j = P_m \cdot m_b \qquad (13)$$

5.1.2 Benefit: Protection from predators (palatability)

Like in ForamEcoGENIE 1.0, calcification protects from grazing and is defined by P_p, which reduces the biomass loss from predation (Eqn. 10).

5.1.3 Cost: higher metabolic cost

We modified the metabolic cost of calcification defined in Grigoratou et al. (2019, 2021a) by replacing the original reduced maximum growth rate (or specifically maximum grazing rate) with a temperature-dependent respiration loss term. We choose this new loss term over a reduced growth rate because (1) extra respiration is a more biologically realistic cost and (2) a temperature-dependent term helps reconcile the low-latitude biomass as observed. The respiration r_j present in Eqn. 5 scales with carbon biomass and is multiplied by constant r_b and temperature limitation (Eqn. 11). We assumed that the lost carbon from respiration is instantly recycled back to DIC pool.

$$r_j = r_b \cdot \gamma_T \qquad (14)$$

5.2 Spine trait trade-offs

Spines are foraminifer's taxonomical basis and are made up of calcite. The biological functions of spines are related to stability in water columns, symbiosis and feeding behaviour (Schiebel and Hemleben, 2017).

5.2.1 Benefit: Enhanced grazing

Studies show that spinose foraminifera are more efficient in capturing and digesting prey thanks to the spine and rhizopodia networks (Anderson and Bé, 1976). Spines widen the prey availability of immotile foraminifer and facilitate capturing larger preys, while non-spinose species cannot hold active prey and only accept smaller particles of copepods in the laboratory observations (Anderson et al., 1979; Hemleben et al., 1989). Grigoratou et al., (2021b) modelled such benefit by reducing the half-saturation constant (conventionally noted as $\boldsymbol{k}$ in a Michaelis-Menten model). Here we adopt this approach by reducing $k_{j_{\text{prey}}}$ by a scaling parameter τ ($0 < \tau < 1$; Eqn. 10).

5.2.2 Other trade-offs as calcification: higher metabolic cost and reduced palatability

Deleted: *1*

Deleted: b

Deleted: .

Formatted: Font: Not Italic

Deleted: 8

Formatted: Font: Not Italic

Deleted: 2.4

Deleted: The link with symbiosis is discussed separately in the following section.

Deleted: *a. Higher metabolic cost and reduced palatability*¶
We assume that the metabolic cost and protection from the spines are characterised the same way as for calcification (Eqn. 10-11), with spinose foraminifera having a higher cost and a stronger protection than non-spinoses (Table 2).¶
¶
b

Deleted: .

Formatted: Font: Not Italic

Deleted: ϵ

Deleted: ϵ

Deleted: 7

Formatted: English (US)

Formatted: Font: Not Italic

We assume that the metabolic cost and protection from the spines are characterised the same way as for calcification (Eqn. 13-14), with spinose foraminifera having a higher cost and a stronger protection than non-spinoses (Table 2). But there is no mortality reduction regarding spine trait.

5.3 Symbiosis trait trade-offs

Deleted: 2.4

Symbiosis is a novel trait in the model, commonly seen in marine organisms including foraminifer. Many planktic foraminifera harbour algae (e.g., dinoflagellate, diatom) within their cell (Takagi et al., 2019). We represent these symbiotic species in the model as a single organism, which combines hetero- and autotrophy, equivalent to a calcifying mixotroph. We use the trait-based representation of mixotrophy of Ward and Follows, (2016), where any plankton can "naturally" predate and photosynthesize, where the alternative strategy for specialist group is turned off (i.e., V_m is 0 for zooplankton and G_m is 0 for phytoplankton), and for mixotrophs turned on.

5.3.1 Benefit: enabled autotrophy for planktic foraminifer

Formatted: Font: Not Italic

The symbiont owns an independent size defined as a symbiont/foraminifera size ratio ψ (Eqn. 16) to characterise the symbiont affinity in taking up nutrients and light. Photomicrograph observations showed that foraminifera symbionts are about 1:20 smaller in size than the host cell (Takagi et al., 2019).

$$V_s = \psi^3 V_h \qquad (15)$$

Formatted: Font: (Asian) +Body Asian (DengXian), Not Italic

The generic nutrient uptake of symbionts follows a mixotrophy- (λ_s), quota- ($Q_{i_r}^{\mathrm{stat}}$) and temperature-limited (γ_T) Michaelis-Menten function where the variable ($\mathbf{R}$) represents nutrient resources and half-saturation constant is replaced by nutrient affinity, a more mechanistic parameter for nutrient uptake α. Nutrient affinity is often referred as "clearance rate" and regarded as a proxy of competitive strength (Fiksen et al., 2013). According to Edwards et al., (2012)' s review on phytoplankton trait trade-offs, scaled nutrient affinity is negatively related to cell size because of lower surface to volume ratio, while maximum uptake rate (V_m) is positively related.

$$\mu_{i_r} = \lambda_s \cdot Q_{i_r}^{\mathrm{stat}} \cdot \gamma_T \cdot \frac{V_{i_r}^m \alpha_{i_r} \mathbf{R}}{V_{i_r}^m + \alpha_{i_r} \mathbf{R}} \qquad (16)$$

The symbionts' photosynthesis growth is modelled following the size-dependent unimodal equation (Geider et al., 1998; Moore et al., 2001), which has shown significant explanatory power for eukaryotes phytoplankton cells than power law (Bec et al., 2008). The maximum photosynthesis rate P_C^m is determined by dimensionless parameter P_a, P_b, P_c and the biovolume of symbiont V_s, and the mixotrophy cost λ_s.

$$P_C^m = \frac{\lambda_s (P_a + log_{10} V_s)}{P_b + P_c log_{10} V_s + {log_{10} V_s}^2} \qquad (17)$$

The practical photosynthesis rate is further constrained by nutrient availability (the smallest between γ_{Fe} and γ_P), temperature (γ_T), light intensity (γ_I).

$$P_C = P_C^m \cdot \min_{[\gamma_P, \gamma_{Fe}]} \cdot \gamma_T \cdot \gamma_I \qquad (18)$$

The nutrient limitation γ_{i_r} (i_r is either P or Fe, see the definition in Eqn. 2) takes the minimal value from phosphorus or iron limitation term, which follows the quota relationship in Droop (1968).

$$\gamma_{i_r} = \frac{1 - Q_{i_r}^{\min}/Q_{i_r}}{1 - Q_{i_r}^{\min}/Q_{i_r}^{\max}}, \quad i_r = \mathrm{Fe, P} \tag{19}$$

As for the light limitation, it follows Moore et al., (2001) model where ***I*** represents light intensity, α is initial slope of P-I curve limited by Fe content (γ_{Fe}), and Q_{Chl} is chlorophyll quota.

$$\gamma_I = 1 - \exp\left(\frac{-\alpha \cdot \gamma_{Fe} \cdot Q_{\mathrm{Chl}} \cdot I}{P_C^m \cdot \gamma_T \cdot \min[\gamma_P, \gamma_{Fe}]}\right) \tag{20}$$

5.3.2 Cost: downgrading autotroph and heterotroph efficiency

The cost of mixotrophy is that both autotrophy and heterotrophy parts (i.e., photosynthesis and grazing rates) are scaled down (by multiplying factor λ_s and λ_h with respect to symbionts and hosts, $0 < \lambda_s, \lambda_h < 1$, Eqn.9 and 16) compared to the pure auto/heterotroph specialist (Ward and Follows, 2016). Despite no direct and sufficient evidence for such a foraminifer predation cost, this assumption is common practice in mixotroph models (Castellani et al., 2013; Våge et al., 2013; Ward and Follows, 2016). We also distinguish between symbiont-obligate and symbiont-facultative foraminifera using different λ_s/λ_h parameter values to reflect their different extent of dependency on symbionts (Table 2).

5.4 Approximating foraminifera calcite export

Planktic foraminifera produce organic carbon in the subsurface water column (Salter et al., 2014) and sequester tests of inorganic carbon into the deep oceans (Schiebel, 2002). In the model the organic carbon flux was consistent as section 3.4. The additional calcite export is approximated by multiplying the foraminifera bulk organic carbon export with a globally uniform particle inorganic carbon (PIC) to organic carbon (POC) ratio, based on the empirical first-order average value (0.36) (Schiebel and Movellan, 2012).

6 Model experiments and evaluation

6.1 Experiments

We run an ensemble of 1,200 model experiments, each testing a different combination of parameter values, to explore all possible trait values and select the best trait combinations to match the foraminifera observations (section 3.2). The parameter sets are generated using Latin Hypercube Sampling (LHS) algorithm, uniformly sampling values of 12 model parameters characteristics of foraminifer traits (Table 2; Sarrazin et al., 2016). Each simulation is run for 250 years continuing from a 10,000-year spin-up simulation as ecosystem structure typically reaches equilibrium after ~50 years. The other ecosystem parameters are the same as Ward et al. (2018) (Table S3).

Formatted: Font: Not Italic

Formatted: Font: Not Italic

Deleted: ¶
We also distinguish between symbiont-obligate and symbiont-facultative foraminifera using different λ_s/λ_h parameter values to reflect their different extent of dependency on symbionts (Table 2).¶
We also distinguish between symbiont-obligate and symbiont-facultative foraminifera using different λ_s/λ_h parameter values to reflect their different extent of dependency on symbionts (Table 2).¶
¶
a. Symbiont cell size¶
We determine the cell size of the symbiont from a defined symbiont/foraminifera size ratio ψ (Eqn. 12) to characterise the symbiont affinity in taking up nutrients and light. Photomicrograph observations showed that foraminifera symbionts are about 1:20 smaller in size than the host cell (Takagi et al., 2019).¶

¶
b. Symbionts' inorganic nutrient uptake¶
The generic nutrient uptake of symbionts follows a mixotrophy- (λ_s), quota- ($Q_{i_r}^{\mathrm{stat}}$) and temperature-limited (γ_T) Michaelis-Menten function where the variable (**R**) represents nutrient resources and half-saturation constant is replaced by nutrient affinity, a more mechanistic parameter for nutrient uptake α. Nutrient affinity is often referred as "clearance rate" and regarded as a proxy of competitive strength (Fiksen et al., 2013). According to Edwards et al., (2012)' s review on phytoplankton trait trade-offs, scaled nutrient affinity is negatively related to cell size because of lower surface to volume ratio, while maximum uptake rate (V_m) is positively related.¶

$V_{i_r} = \lambda$

c. Symbionts' photosynthesis¶
The symbionts' photosynthesis growth is modelled following the size-dependent unimodal equation (Geider et al., 1998; Moore ... [3]

Deleted: 2.5

Deleted: **carbon production and**

Deleted: we estimate

Deleted: and

Deleted: approximate

Deleted: using an empirical converting factor (Schiebel and Movellan, 2012) as previous model implementations (Grigoratou et al., 2021a).

Formatted: English (US)

Deleted: ¶
2.5.1 Organic Carbon Export¶ ... [4]

Deleted: 3

Deleted: 3

Deleted: We set up the model plankton ecosystem to resolve eight size classes of phytoplankton, seven size classes of zooplankton and one size class for each of the four foraminifer groups. Phytopl ... [5]

Deleted: ¶
We use a

Deleted: to generate the 1,200 parameter combinations

Table 2 List of the foraminifer-relevant parameters tested in the global sensitivity analysis (GSA) and identified optimal parameter values for each group

Related trait(s)	Parameter	Description	Tested range†	Unit	Optimal values* (bn)	Optimal values* (bs)	Optimal values* (sn)	Optimal values* (ss)
Calcification/spine	p_m	Protection from mortality	[0-1]		0.6	0.6	0.6	0.6
	p_p	Protection from palatability	[0-1]		0.8	0.7	0.8	0.7
	r	Respiration rate	[0-0.02]	mmol C d^{-1}	0.04	0.06	0.04	0.06
Spine	τ	coefficient of grazing half saturation	[0-1]		/	0.9	/	0.9
Symbiosis	ψ	symbiont to foraminifer size ratio	[0-0.05]		/	/	0.0015	0.0015
	λ_s	symbiont autotroph efficiency	[0-1]		/	/	0.2	0.8
	λ_h	foraminifer heterotroph efficiency	[0-1]		/	/	0.8	0.55

bn, symbiont-barren non-spinose; bs, symbiont-barren spinose; sn, symbiont-facultative non-spinose; ss, symbiont-obligate spinose

* For any other plankton group without these traits, scaling parameters are set to 1 and cost parameters are set to 0.

† GSA range is set to [0-1] for scaling parameters; respiration terms are as follow Ward et al., (2018); symbiont cell size ratio upper bound is calculated from observation (Takagi et al., 2019).

6.2 Comparison to observations

The model generates biomass, export production for each group, and relative abundance is estimated based on export production. To validate these model outputs, we compiled 3 global adult foraminifer (>150 µm) datasets: (1) plankton net tows mostly taken from the first 100 m, (2) sediment core-top representing the Late Holocene (pre-industrial) and (3) seasonally resolved sediment trap time-series. We use the core-top dataset of individual abundance count to validate the spatial patterns of the relative abundance of each foraminifer group. The plankton net tow datasets are used to validate the living stocks. And the sediment trap data are used to compare with foraminifer-derived carbon export. The core-top data comes from ForCenS (Siccha and Kucera, 2017), and the plankton tow and sediment trap data from the compilation by Grigoratou, (2019) with additional foraminifera groups and sample sites. The full list of plankton tow and sediment trap data sources is in Tables S1 and S2.

For all the datasets, we firstly sum species into functional groups using species traits defined by Schiebel and Hemleben, (2017) and Takagi et al., (2019) (Table S4). Next the sediment trap and plankton tow data are taken annual average for spatial comparison. We also regrid the observations to be consistent to our model, which means that all the observations within a grid are averaged. Finally, we use Mielke measure (next section) to quantify the model-data fit. Note (1) this is for spatial comparison and therefore we do not take annual average and calculate skill scores for seasonal model-data comparison (2) the

Deleted: for the best model run

Formatted: Right: -0.37 cm

Formatted: Right: -0.38 cm

Formatted: Right: 0.4 cm

Formatted Table

Formatted Table

Formatted: Font: 9 pt

Deleted: Foraminifer group* ... [6]

Deleted: 3

Formatted: Font: Not Bold

Deleted: ¶

Deleted: the

Deleted: foraminifera model

Deleted: three

Deleted: datasets of

Deleted: data

Formatted: Font: Not Bold

Deleted: sediment

Deleted: proportion

Deleted: We also use t

Deleted: ocean

Deleted: (count m^{-3})

Deleted: and sediment trap (count m^{-3} d^{-1})

Deleted: a

Deleted: carbon

Deleted:

Deleted: of each group, respectively

Arctic and the Mediterranean Sea are omitted in comparison because of the resolution-derived model's poor ocean physics in those regions.

The units of plankton net tow ("count m^{-3}") and sediment trap data ("count m^{-2} d^{-1}") are converted into "mmol C m^{-3}" and "mmol C m^{-2} d^{-1}" using the empirical factor of 0.845 μg $count^{-1}$ from Schiebel and Movellan (2012). The model generates carbon export production in "mmol C m^{-3} d^{-1}", so it is transformed to "mmol C m^{-2} d^{-1}" by multiplying the surface layer depth (80.8 m). Note that although the sediment traps were deployed in different depths (averagely 1.96 km) and seasons. we ignore the vertical degradation because foraminifer tests are relatively fast-sinking due to large size (Takahashi and Be, 1984) and we do not have well-built attenuation profile for foraminifer tests.

We considered species with less than 3% abundance as absent to avoid the uncertainty caused by ocean currents transportation (van Sebille et al., 2015). We applied this threshold based on the standard error of fisher's α diversity index (Fisher et al., 1943).

6.3 Performance metrics

We use Mielke measure, or M-score (Watterson, 1996; Watterson et al., 2014) to quantify the model-data fitting goodness (Eqn. 21). This metric is essentially non-dimensional transformed mean square error, and has been widely used in general circulation models (Gregoire et al., 2011, Anon, 2016). This score spans from -1 to 1 with values closer to 1 representing better model performance, 0 stands for no predicting skills. And negative M-score indicates negative correlation.

$$M = \frac{2}{\pi} arcsin \left[\frac{\sum_{i=1}^{n} (M_i - O_i)^2 / n}{\sigma_m^2 + \sigma_o^2 + (\mu_m - \mu_o)^2} \right] \tag{21}$$

The numerator is mean square error, with M_i and O_i the model and observational value in the i^{th} grid, and n the total number of grids. σ^2 and μ are the variance and mean, with superscripts m and o representing model and observed fields, respectively.

6.4 Global Sensitivity analysis

We conduct a global sensitivity analysis (GSA) to explore the model robustness of our 1,200 experiments using the PAWN method (Pianosi and Wagener, 2015). This method measures the sensitivity of model outputs (focusing on M-score here) to different values of input parameters. A total M-score is calculated by summing scores of each foraminifer group in biomass, POC export, and relative abundance (i.e., the total score ranges from -12 to 12). To further measure the uncertainty and robustness of the GSA results, we also apply a bootstrapping method with 1,000 resamples. This method allows us to understand the confidence intervals of the sensitivity indices without running more experiments (Wagener and Pianosi, 2019). We bootstrapped our data using *rsample* package (Silge et al., 2021) in the R software environment v4.1 (R Core Team, 2021).

7 Results and discussions

7.1 Model ensemble results

Formatted: (Asian) Chinese (China), (Other) English (US)

Deleted: We converted t

Deleted: from "count m^{-3}

Deleted: " or

Deleted: ^{3}

Deleted: or

Deleted: ^{3}

Formatted

Deleted: To further constrain the uncertainty of the observational data, we applied median absolute deviation (MAD) measurement to detect the most robust and close-to-reality data. Finally, we grouped the species-based data into functional groups (Table 1) using species traits defined by Schiebel and Hemleben, (2017) and Takagi et al., (2019) (Table S2).

Deleted: To compare with the sediment-trap and plankton tow time-series, we select sites with the most data points. For the time slice comparison, we re-gridd the observational data by averaging data in each model grid box. ¶
We also perform basic statistics (mean, standard error, sum) on the model and observational data. We use the standard error of the mean to represent the accuracy of the sampling mean, particularly for the observational studies. Finally, we do not consider model outputs for the Arctic and the Mediterranean Sea because of limitations with ocean physics due to low model resolution in that region.¶

Deleted: 3

Formatted: English (US)

Deleted: calculate

Deleted: a

Deleted: (Watterson, 2015) for each model experiment

Deleted: 19

Formatted: (Asian) Chinese (China), (Other) English (US)

Deleted: *1*

Deleted: 3

Deleted: flux

Deleted:),.

Deleted: 4

Deleted: 4

Overall, the 1,200 model runs fit generally reproduce POC export (summed M-score: -0.2 ~ 1.0) and relative abundance (summed M-score: -0.5 ~ 1.2), with poorer comparison with plankton net data (summed M-score: -0.1 ~ 0.5) (Figure 2). A heatmap of M-Scores (Figure 2) shows the experiments cluster into 4 groups with respect to the 3 observation metrics. Most parameter combinations (cluster C) show low performance in predicting foraminifer metrics. Cluster D shows an inverse relative abundance distribution to the observation, while cluster B has only good POC export performance. Cluster A which includes our optimal parameters achieves the highest (best) abundance M-score and has good biomass and POC export prediction. We notice that this cluster accompanies low foraminifer export production, which indicates that the higher-than-observation biomass/carbon are the primary constrain for the model to get better scores. The sensitivity analysis result confirms this. Our model performance is mostly sensitive to the symbiosis efficiency (λ_s), and the palatability protection (P_p) from both spine and calcification which both directly govern the nutrient uptake and loss (Figure 3). Models with low export production and higher scores associate with <200 µm foraminifer size and small symbiont size (symbiont/host size ratio <0.02) which facilitate dwelling in the tropical regions, realistic shell protections and high respiration cost that do not lead to striking biomass/export (Figure S3).

We select the optimal parameter set with the highest total M-score score (Table 3), which also has the highest M-score for the relative abundance (group mean = 0.3) and POC export (group mean = 0.16; Figure S1). In this run, all the foraminifera groups achieve the highest total M-score (Figure S2). More details about this optimal model is shown in next sections.

Deleted: 4

Deleted: 4

Deleted: 4

Deleted: 14

Deleted: 2

Deleted: 2

Deleted: 5

Deleted: Most clusters

Deleted: (A-D)

Deleted: trade-off between relative abundance and POC export performance, with either higher POC flux score but lower abundance score (cluster A, D), or *vice versa* (cluster C).

Deleted: E

Deleted: (

Deleted: our best run

Deleted:)

Deleted: and

Deleted: POC export scores while showing the closest export rate to observations

Deleted: .¶

Deleted: run

Deleted: 29

Deleted: flux

Deleted: 18

Deleted: Figure S1

Deleted: We prioritise a higher score in relative abundance over POC flux and biomass because of better data quantity and quality in the top-core dataset.

Deleted: except the symbiont-facultative non-spinose have

Deleted: Table

Deleted: 3

Deleted: Compared to the EcoGENIE and ForamEcoGENIE 1.0, this set of parameters does not increase the overall ecosystem biomass or POC export, and slightly increases the mean cell size by ~0.5 µm (Figure 3c). Therefore, the incorporation of symbiosis and spines into our trait-based model successfully widens the ability of the model to represent foraminifers in the surface ocean by incorporating all four main foraminiferal ecogroups in the modern ocean without weakening the overall ability of predicting ecosystem body size, biomass and POC export.

Formatted: English (UK)

Formatted: Centred

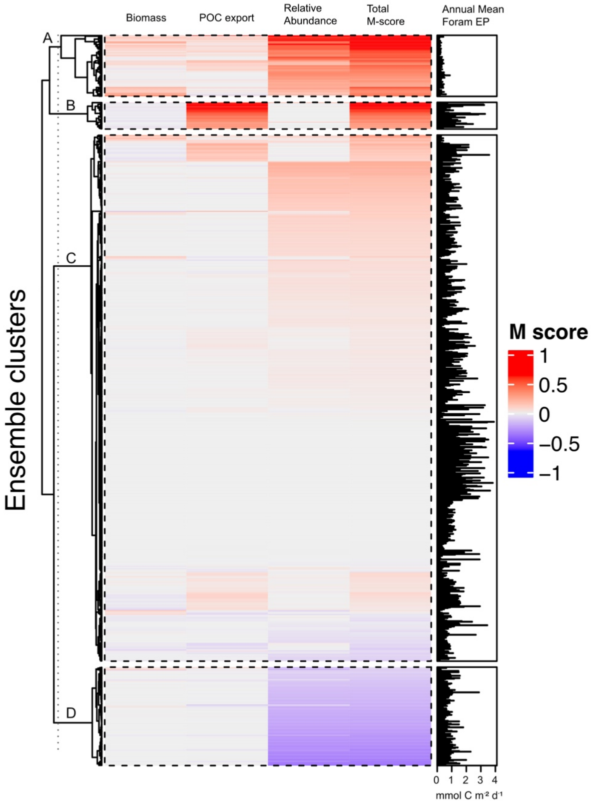

Figure 2. M-score heatmap of the model ensemble compared with foraminifera “Biomass” (plankton net data), “POC export” (sediment trap data), groups’ “Relative Abundance” (sediment core top data). Each column sums the M-score of four foraminifer groups, and the fourth column is the sum of all the left three. The right panel shows the global annual mean export production of all foraminifer groups. The ensemble cluster was derived from a complete linkage clustering algorithm (Jarman, 2020). The higher the M-score value the better the performance, negative value stands for negative correlation.

Deleted: 2

Deleted: flux

Deleted: relative

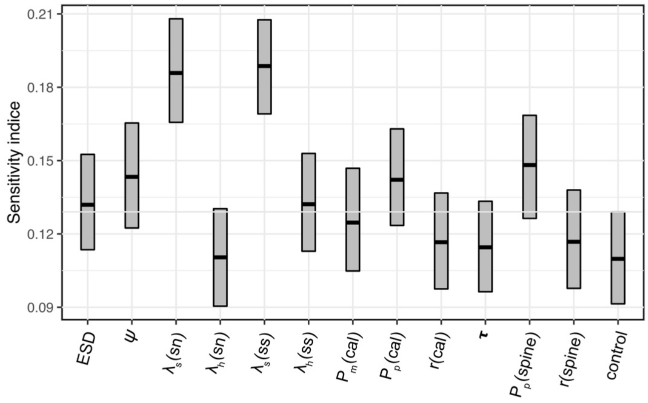

Figure 3. Sensitivity of parameters to overall model performance (as summed M-scores). Bar boundaries indicate the 95-percent confidence interval with the thick line showing the mean value. Grey line indicates non-influential upper limit of index value as control group. sn, symbiont-facultative non-spinose; ss, symbiont-bearing spinose. cal, the abbreviation of calcification. τ is the spine effect on grazing rate

Table 3. The distribution of M-scores across foraminiferal groups from the optimal parameter set

Groups	Symbiont-barren non-spinose	Symbiont-barren spinose	Symbiont-facultative non-spinose	Symbiont-obligate spinose	Column sum
Biomass	0.19	0.08	-0.05	-0.05	0.17
POC Export	0.11	0.07	0.43	0.02	0.63
Relative Abundance	0.51	0.35	0.02	0.32	1.20
Row sum	0.81	0.50	0.40	0.29	2.00

7.2 Relative abundance distribution of foraminifer groups

Our model with optimal parameters compares reasonably well with observations of core-top data showing the relative spatial distribution of the four foraminifera functional groups (Figure 4). The presence/absence pattern is also captured well in

Formatted: Centred

Deleted: ¶

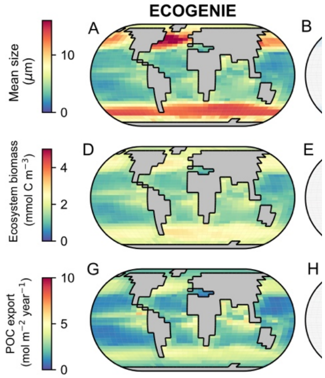

Deleted: ... [7]

Deleted: Best model run for M-scores…he distribution of M ... [8]

Formatted: Font: 8 pt

Formatted: Right: -1.41 cm

Formatted Table

Deleted: mean

Formatted: Font: 8 pt

Deleted: 00

Deleted: 00

Deleted: 0

Deleted: 0

Deleted: 00

Formatted: Font: 8 pt

Deleted: 19

Deleted: 28

Deleted: 09

Deleted: 15

Deleted: 18

Formatted: Font: 8 pt

Deleted: 42

Deleted: 31

Deleted: 05

Deleted: 38

Deleted: 0.29

Formatted: Font: 8 pt

Deleted: Mean

Formatted: Font: 8 pt, English (US)

Formatted: Font: 8 pt

Deleted: 20

Deleted: 30

Deleted: 05

Deleted: 0.18

Deleted: ¶ ... [9]

Deleted: 4

Deleted: best…model run …ompares reasonably well with ... [10]

sediment trap and plankton net studies (Figure 4,5). The symbiont-obligate spinose group is the most abundant group with a global relative abundance of 60.7% (M-score: 0.32, Figure 4g) dominating in the tropical open oceans, while the symbiont-barren non-spinose (Figure 4a) and spinose groups (Figure 4c) both mainly occupy the high latitudes (M-score = 0.51 and 0.31, respectively). The symbiont-facultative group (Figure 4e) is underestimated with the visible model-data disparities in the eastern equatorial pacific where the sediment core shows exclusively high abundance. This may be due to the resistant dissolution of some species' test (e.g., *N. dutertrei*) as suggested in a previous model study (Lombard et al., 2011). Overall, the Root Mean Square Error (RMSE) of relative abundance in this model (12% to 42%, Table S5) is comparable to the species-based models, like FORAMCLIM (5-23%, Lombard et al., 2011) and PLAFOM (22-25%, Fraile et al., 2009). This indicates that symbionts and spines are sufficient to explain the variance of geographic distribution.

While non-symbiotic foraminifer follows the biogeography of prey in high nutrient areas, the symbiont size (0.0015 symbiont/foraminifer) indicates that the small body size and therefore high nutrient affinity is a key factor for symbiotic foraminifer in low-nutrient areas like subtropical gyres. Although this actual symbiont size does not necessarily be around 0.0015 times foraminifer size, the fact that foraminifer can host up to 3,000 algal cells can explain the high nutrient uptake efficiency (Spero and Parker, 1985). The symbiont-barren spinose foraminifer (Figure 4d) displays higher abundance in Arabian Sea, South China Sea than non-spinose foraminifer (Figure 4b). This might be related to the carnivory feeding (rather than enhanced grazing efficiency) of spinose foraminifer that is not included in current model.

Deleted: 5

Deleted: 6

Deleted: 43.2

Deleted: 0.38

Deleted: 0.42

Deleted: 0.31

Deleted: is not well captured

Deleted: 12

Deleted: 32

Deleted: S3

Formatted: (Asian) Chinese (China), (Other) English (US)

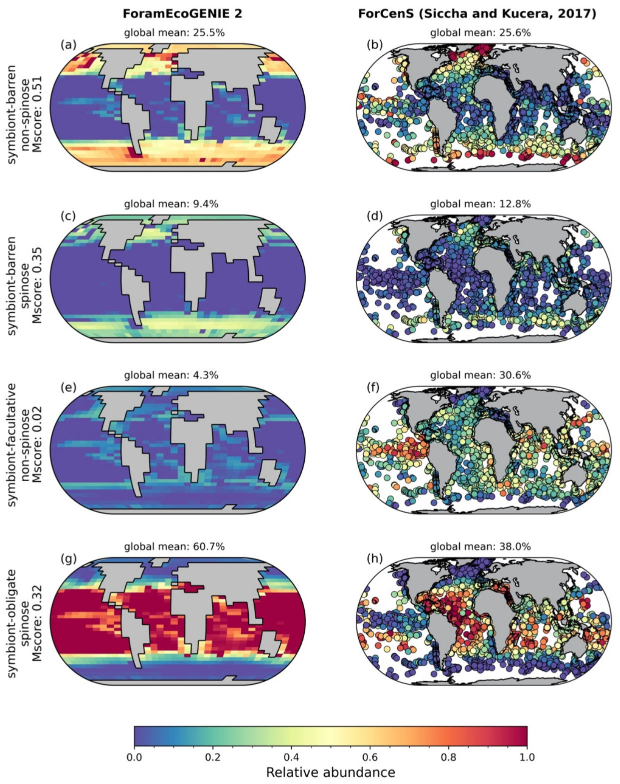

Figure 4. Relative abundance of the modelled geographical distribution (left column) of the four planktic foraminifer function groups, compared to the ForCenS core-top dataset (right column; Siccha and Kucera, 2017). Subplots titles are the M-scores derived relative to observation and the global mean of relative abundance.

7.3 Annual average biomass of foraminifera groups

As the plankton tow data, the model reproduces the low biomass of planktic foraminifer (Figure 5). The global annual mean of biomass ranges from 0.001 to 0.010 mmol C m^{-3}, or 0.08-0.8 mmol C m^{-2}, with the most contribution from symbiont barren groups (Figure 7). Globally integrating all foraminifer groups, the model estimates 0.0068 Gt C or 6.83 Tg C biomass (Figure 7). For comparison, the MAREDAT project estimated the global average biomass of 0.24-0.94 mmol C m^{-2} which integrates

Deleted:

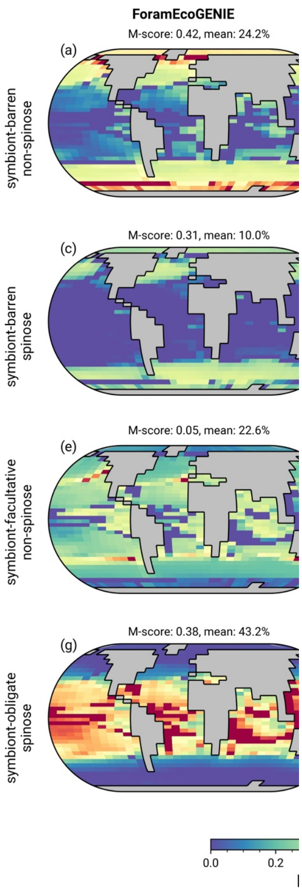

Deleted: 4.… Relative abundance of the modelled geographical distribution (left column) of the four planktic foraminifer function groups, compared to the ForCenS core-top dataset (right column; Siccha and Kucera, 2017). Subplots titles are the M-scores derived relative to observation and the global mean of relative abundance. Model relative abundance of each group are calculated based on POC flux rates. ... [11]

Deleted: 4.…3 Annual average Living b ... [12]

Formatted ... [13]

all the depth from 0 to 2,500 m (Schiebel and Movellan, 2012). Schiebel and Movellan (2012) also estimated a total of 0.94~3.63 Tg C living foraminifer at any time point. Given the similar mean biomass range estimation, the difference of total biomass between our model and this data is likely caused by the grid area estimation. Therefore, it is safe to state that the model produces good estimation compared with the observation.

The skill score, however, does not capture this good mode-data fit. This is mostly caused by regridding the data points into model grid resolution. The plankton net data are spatially concentrated in North Atlantic, Northwestern Pacific, Arabian Sea, and Indian sector of Southern Ocean. Under such circumstance, regriding causes sparser data and makes skill score sensitive to several outlier grids. Therefore, the insufficient data is the major reason of low scoring in biomass.

Formatted: Superscript

Deleted: Although the general distribution pattern of foraminifera living biomass agrees with the observations from plankton nets (Figure 4), the corresponding M-scores are close to 0, indicating the model's inability in reproducing the living biomass magnitude of plankton net data. Our model overestimates the observed biomass on average by 0.02 mmol C m^{-3} (Figures 5 and 7a) or around 8 times. The model estimates a total of 32.3 TgC foraminifer organic carbon biomass, with symbiont-barren non-spinose taxa contributing the most (32.1%, or 10.3 TgC) (Figure 3c). For comparison, the MAREDAT dataset estimated the global mean living biomass of 0.0024 mmol C m^{-3} and the total of 0.94~3.63 TgC living foraminifer (with all groups included), with the production rate of 8.2–32.7 TgC yr^{-1} (Schiebel and Movellan, 2012). This indicates more foraminifer biomass are grazed by higher trophic levels than the model predicts because of the generally higher carbon export rate particularly for non-spinose foraminifera (Figure 7; see next section).

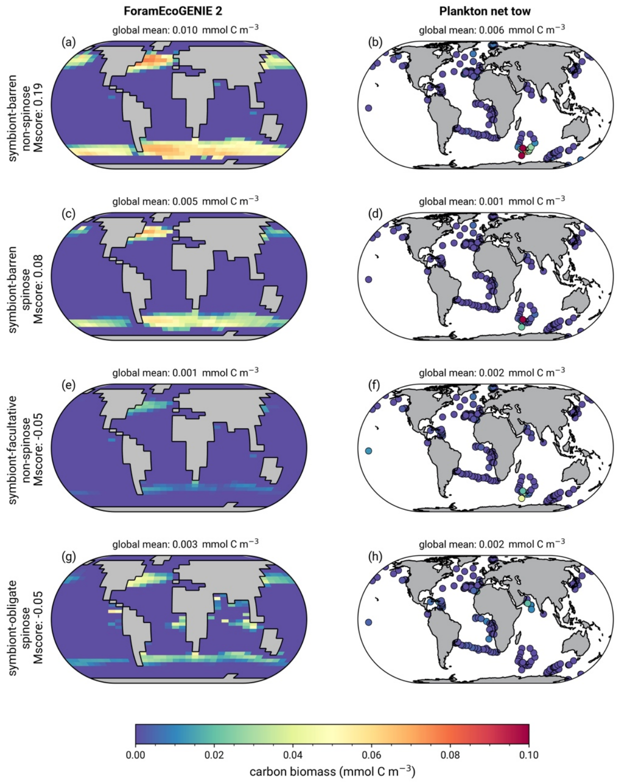

Figure 5. Model outputs of annual average biomass (mmol C m^{-3}) compared with plankton net data (right column) for the four main functional groups of planktonic foraminifera.

7.4 Annual average POC and calcite export of foraminifera groups

The model reproduces consistent geographical distributions and magnitude of POC export compared to sediment trap samples for all 4 foraminifer groups (Figure 6, 7). The model estimates 0.002-0.031 mmol C m^{-2} d^{-1}, compared with 0.001-0.026 shown in sediment trap studies. However, the total M-score for the model POC export is 0.63, not reflecting the good matchiness between model and observation. This is similarly caused by limited data as previous biomass section.

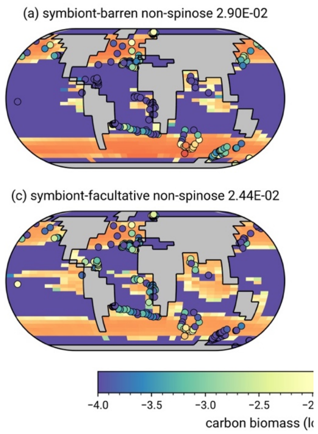

Deleted:

Deleted: 5

Deleted: living

Deleted: in log-10 scale

Deleted: dots

Formatted: English (US)

Deleted: 4.

Deleted: fluxes

Deleted: 6

Deleted:). The modelled mean POC flux rate is close to the collected trap observations for spinose foraminifers (Figure

Deleted: 7

Deleted: but overestimates the POC flux of non-spinose foraminifer ~4 times

Formatted: Superscript

Formatted: Superscript

Formatted: Not Superscript/ Subscript

Deleted: T

Deleted: mean

Deleted: flux

Deleted: around

Deleted: 0.2

Deleted: , with the symbiont-baren spinose group performing the best (0.28) and the symbiont-facultative group performing th ... [14]

In terms of global estimation, the model suggests the foraminifer-derived organic carbon export of 0.1 Gt C yr^{-1}. Symbiont-barren non-spinose taxa dominate this carbon export (55%) followed by symbiont-barren spinose, symbiont-facultative and symbiont-obligate groups (30%, 3% and 11% respectively). Integrating all the ecogroups and using an empirically averaged PIC:POC ratio of 0.36 (Schiebel and Movellan, 2012), our model estimates a total calcite flux of pelagic foraminifera of 0.033 Gt PIC yr^{-1} (Figure 8), which is at least five times smaller to the 0.16–0.39 Gt PIC yr^{-1} of Schiebel (2002) within the top 100-m ocean. The reason is likely we calibrate the model with sediment traps deployed in averagely 2 km water, while the high flux signal in the top 300 m is not captured. In addition, the high temporal variability in the observation is also not well captured by the model.

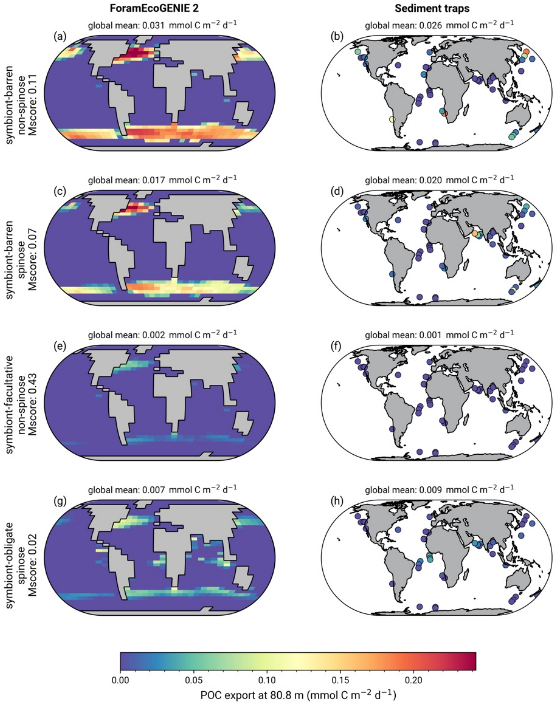

Deleted: 365.3

Deleted: Tg

Deleted: 141.7 TgC yr^{-1}

Deleted: 93.2

Deleted: 83.1

Deleted: 47.3 TgC yr^{-1},

Deleted: U

Deleted: converting mass ratio of 1:3 from organic carbon to calcium carbonate

Deleted: 1.1

Deleted: $CaCO_3$

Deleted: comparable

Deleted: 1.3-3.2

Deleted: The calcite export in the model falls within the low range of previous estimates (1.3-3.2 Gt yr^{-1}; Schiebel et al., 2001) and contributes 19% to the global marine $CaCO_3$ production (Milliman et al., 1999). This estimate is similar to 21% reported in Kiss et al., (2021) based on sediment traps at Cape Blanc and to Salmon et al., (2015) data from the Sargasso Sea ranging between 0-40 % (but mostly < 25%). Regionally higher contributions (32-49%) have been reported in the Southern Ocean (Salter et al., 2014) who included deep-dwelling species which are not represented in this model. To summarise, our estimation of foraminifer calcite export is generally trustable to previous observational studies.

Deleted: ¶

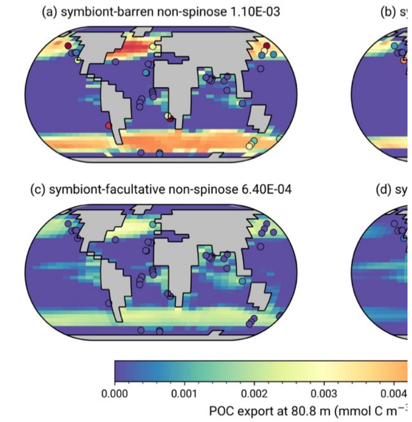

Figure 6. Model outputs of annual average POC export (mmol C m^{-2} d^{-1}) below the euphoric zone (80.8 m) in comparison to sediment trap samples (right column).

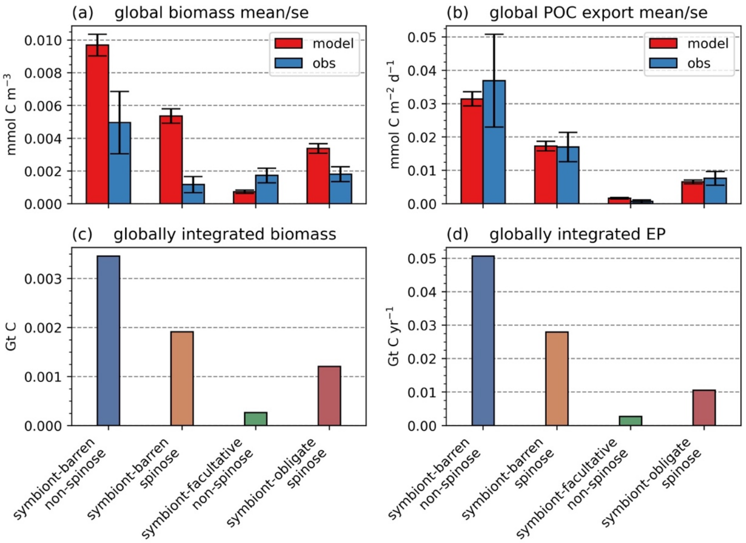

Figure 7. Summary of the modelled annual average biomass and POC export produced by the four foraminifer groups. (a) The modelled (red) and observational (blue) biomass (mmol C m^{-3}) and (b) POC export below the euphotic zone (mmol C m^{-3} d^{-1}). Bar height and error bar represents spatial mean value and standard error, respectively. (c) A global estimation of modelling globally integrated carbon biomass (Gt C) and (d) export production (EP, Gt C yr^{-1}).

Deleted: 6

Deleted: flux

Deleted: ^{3}

Deleted: dots

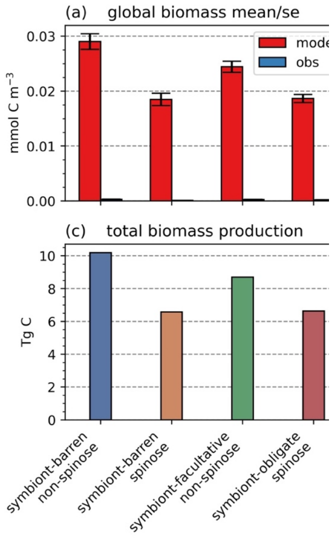

Deleted:

Deleted: 7

Deleted: living

Deleted: flux

Deleted: rate

Deleted: total

Deleted: Tg

Deleted: POC export rate

Deleted: TgC

Formatted: English (US)

Deleted: Compared to the EcoGENIE and ForamEcoGENIE 1.0, this set of parameters does not increase the overall ecosystem biomass or POC export, and slightly increases the mean cell size by ~0.5 µm (Figure 3c). Therefore, the incorporation of symbiosis and spines into our trait-based model successfully widens the ability of the model to represent foraminifers in the surface ocean by incorporating all four main foraminiferal ecogroups in the m ... [15]

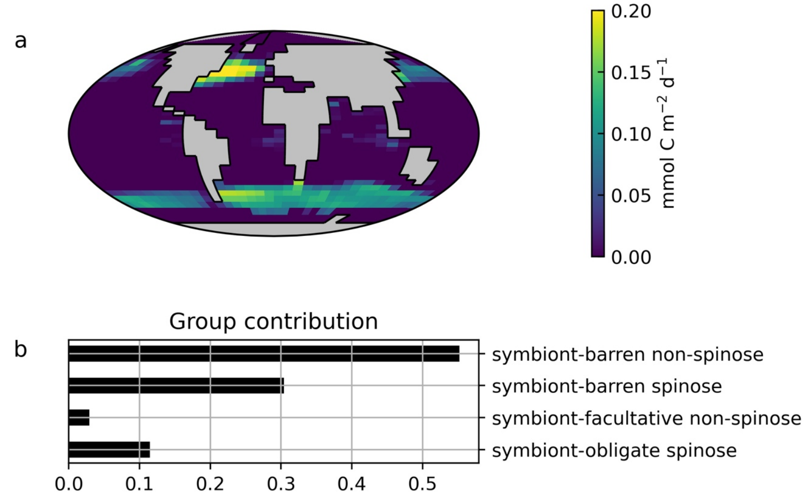

Figure 8 Global model estimates of (a) surface foraminiferal calcite flux (at 80.8 m; mmol C m^{-2} yr^{-1}) and (b) group contribution.

7.5 Seasonal variations of foraminifera biomass and POC export

The model-derived seasonality of foraminifera biomass and POC export are compared with observations in Figure 9 and 10. In terms of seasonal amplitudes, the model fails to show the peakiness in upwelling regions such as Arabian Sea and Ross Sea. This pattern that observational amplitude is stronger than model is also shown in PLAFOM 2.0 (Kretschmer et al., 2018). In contrast, the low export and seasonality in open ocean locations such as the western Atlantic and the Sargasso Sea are better captured. For the seasonal pattern (peak time), foraminifer maximum export production in the polar regions (e.g., Subantarctic zone) happen in winter and our model agrees with this. In most tropical to temperate oceans, both the model and observation show summer/autumn peak time, but offset might exist. For example, the BIOTRAN station see highest biomass in April, while the model predicts July.

The sediment trap observations also indicate the group-specific seasonal cycle difference. Jonkers and Kučera, (2015) summaries foraminifer into warm group, cool and temperate group, and deep dwelling group according to their seasonal cycle patterns. The warm group (i.e., the symbiont-bearing group) shows peak times mostly in September, while cool/temperate group's (non-symbiont groups) peak times concentrate in January to April. Similar group-specific difference in the model was

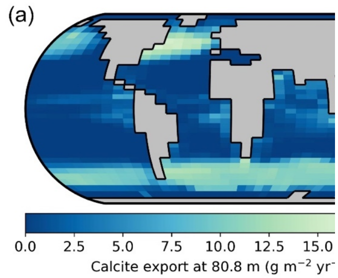

Deleted:

Formatted: English (US)

Deleted: 8

Deleted: flux rate

Deleted: g

Deleted: 4

Deleted: living

Deleted: ¶

Deleted: T

Deleted: successfully reproduces the first-order

Deleted: seasonal patterns observed by sediment trap data at a basin scale,

Deleted: with

Deleted: , summer blooms in the low latitudes (NW Pacific, Ocean Papa Station, Bay of Bengal) and spring blooms in high latitude (Subantarctic Zone).

Formatted: (Asian) Chinese (China), (Other) English (US)

Deleted: (

shown in Figure 11. In addition, the cool/temperate group's earlier-when-warmer signature is also well reproduced in our model from high to low latitude. However, some detailed patterns like the occasionally two cycle per year is not shown in the model. Overall, the model reproduce the seasonal peak time well for different groups, despite the weaker amplitude than the sediment traps suggest.

The foraminifer intra-annual biomass/export variability are driven by the seasonal environmental changes which determine how optimal foraminifera are in the ecological niche. Usually, temperature is assumed as the primary driver. However, the correlated factors like primary productivity are likely to be the true driver (Jonkers and Kučera, 2015). This might be the reason why our model cannot produce as high production as the sediment traps because the upwelling regions in GENIE model are relatively poor constrained. In addition to the model, the low spatial and temporal resolution of observed data also limits us to have a broader overview of seasonal variation, especially in the term of biomass. We also suggest that more functional trait studies regarding temporal variability such as dwelling depth, life history cycle should help resolve this gap in the future.

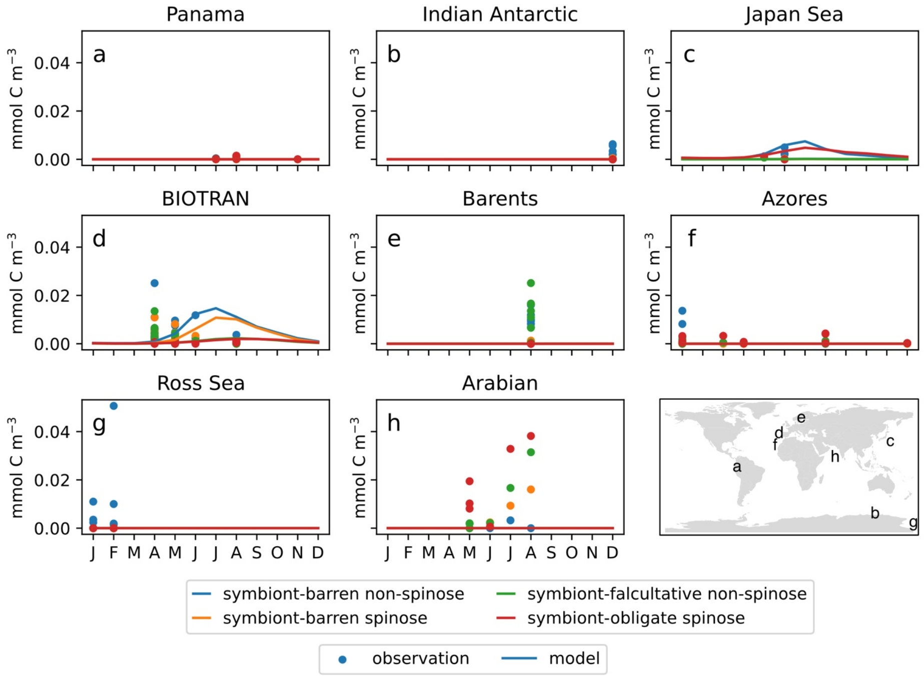

Deleted: (Fraile et al., 2008)

Formatted: English (US)

Deleted: These results are generally consistent with PLAFOM (Fraile et al., 2008) despite species-specific discrepancy. The model does not reproduce biomass change in some upwelling and polar regions (e.g., Arabian Sea, Ross Sea) likely due to the low model resolution.¶

Deleted: ¶
An additional source of uncertainty is the data quality, as ideally models should be calibrated against spatially and temporally abundant and well-constrained data. Therefore, the comparison of our model against plankton tow data was limited by the low temporal resolution of the data (Figure 9). The data is not only undersampled in limited regions (North Atlantic Ocean, Caribbean, Sea Arabian Sea) but also biased towards specific sampling seasons, generated using different mesh size and water depth as discussed in the first application of ForamEcoGENIE (Grigoratou et al., 2021a)

Deleted: ¶
Parameter sensitivity test¶
¶
We conducted a sensitivity analysis to determine which parameters influence the model performance most. The results show that the model performance is mostly sensitive to the symbiosis trait (λ_s), and the palatability protection (P_p) from both spine and calcification (Figure 10), confirming the important role of symbiosis and protection from predators in foraminiferal ecology and the p ... [16]

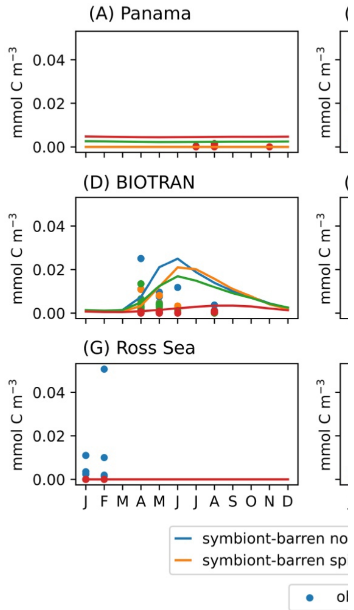

Deleted:

Figure 9. Biomass seasonal comparison between the model (lines) and plankton net tows (dots) (mmol C m^{-3}) in example locations (shown in the map with corresponding letter). Sites are selected to according to the number of comparable data points and ocean basins.

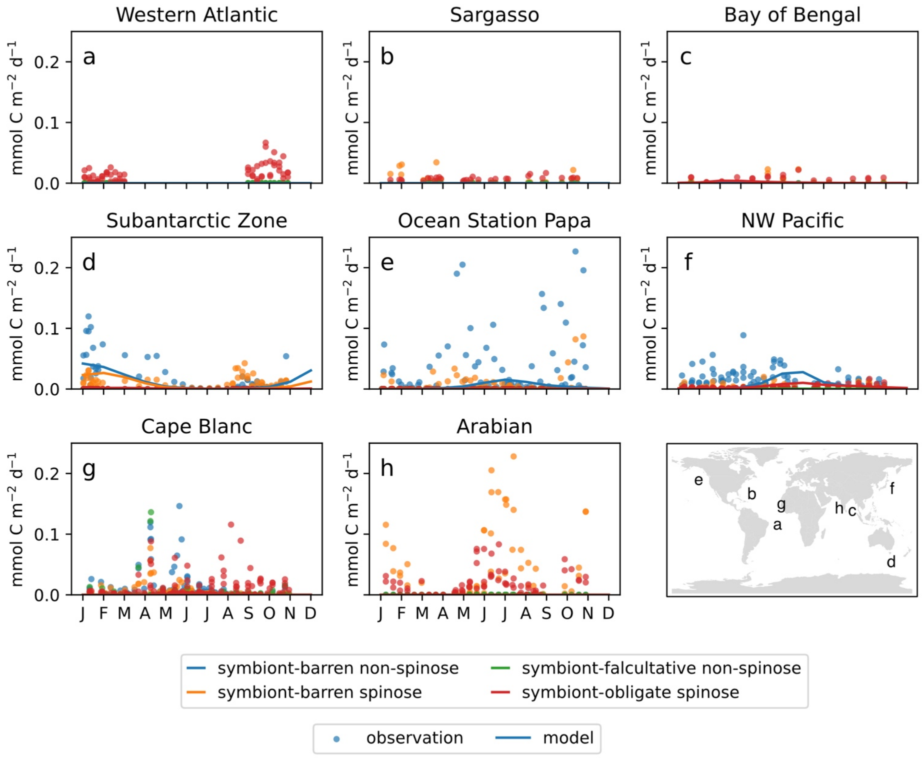

Figure 10. POC export seasonal comparison between the model (lines) and sediment traps (dots) (mmol C m^{-2} d^{-1}) in example sites (shown in the map with corresponding letter). Sites are selected to according to the number of comparable data points and ocean basins.

Deleted: 9

Deleted: observations

Formatted: English (US)

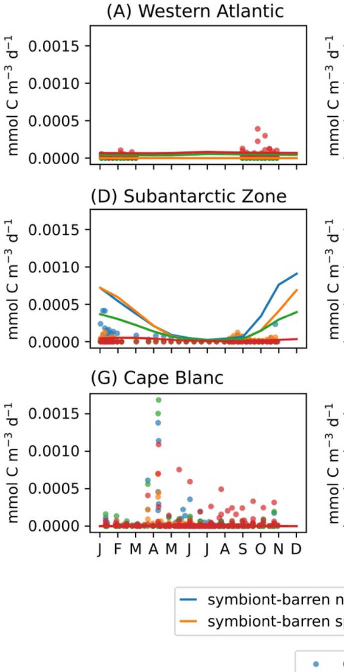

Deleted:

Deleted: 10

Deleted: flux

Deleted: observations

Deleted: ^{3}

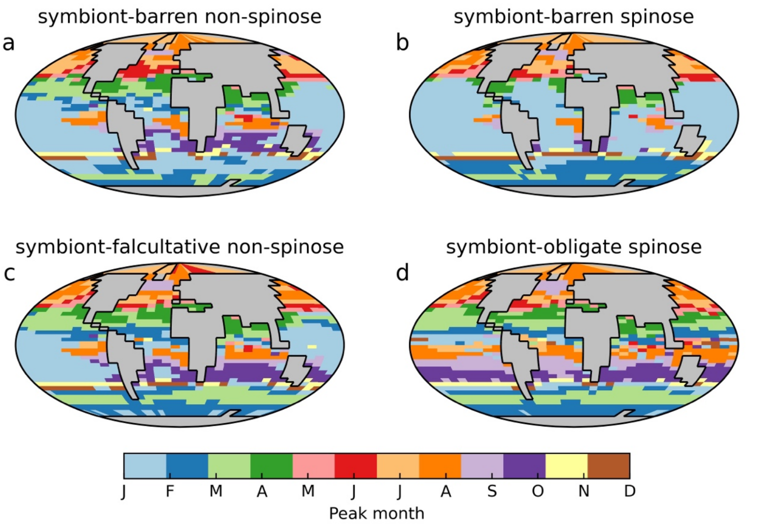

Figure 11. The peak month of modelled biomass annual time series of each foraminifer group.

8 Comparison to prior model iterations

Compared to the EcoGENIE and ForamEcoGENIE 1, the introduction of more foraminifera groups expands the ecosystem mean body size in the tropical and subtropical regions due to their large shell of 190 µm (Fig. 12c). This is mostly caused by the symbiont-bearing groups which fit the warm niche. In contrast, the biomass sees a small change to the whole ecosystem because foraminifer's low standing stocks. NPP and POC export show decreasing changes in the polar regions. And the trends are understandable by adding more grazers. Overall, ForamEcoGENIE 2 slightly magnify the signal of ForamEcoGENIE 1, but these changes are small in biomass/POC export/NPP. Therefore, the incorporation of symbiosis and spines into our trait-based model successfully widens the ability of the model to represent foraminifera community without weakening the overall ability of predicting ecosystem and biogeochemical attributes.

Although ForamEcoGENIE 2 development focuses on the marine ecology, it also lays the foundation to future linking to biogeochemical cycles. For example, spinose foraminifer has more calcite export than non-spinose foraminifer and spines

Formatted: Left

Deleted: **Parameter sensitivity test**
(Selosse et al., 2017)

Deleted:
We conducted a sensitivity analysis to determine which parameters influence the model performance most. The results show that the model performance is mostly sensitive to the symbiosis trait (λ_s), and the palatability protection (P_p) from both spine and calcification (Figure 10), confirming the important role of symbiosis and protection from predators in foraminiferal ecology and the possibility that overestimated biomass of non-spinose foraminifer is influenced by the palatability parameterisation.

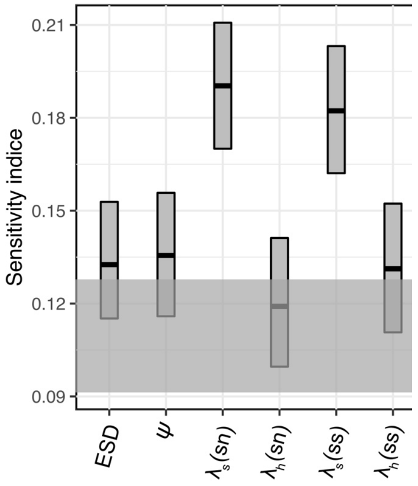

Figure 11. Sensitivity of parameters to overall model performance (as combined M-scores). Bar boundaries indicate the 95-percent confidence interval with the thick line showing the mean value. Grey area indicates non-influential range of index value as control group. sn, symbiont-facultative non-spinose; ss, symbiont-bearing spinose.

control the sinking velocity of foraminifer shell (Takahashi and Be, 1984). Symbiotic groups expand the global niche for foraminifer. The community compositional change of these groups under different climatology would influence the ocean carbon cycles by changing the calcite export and surface alkalinity. So far, no Earth system models have explicit foraminifer group participating the inorganic carbon cycle. Therefore, this would be an important direction of our model development in the future.

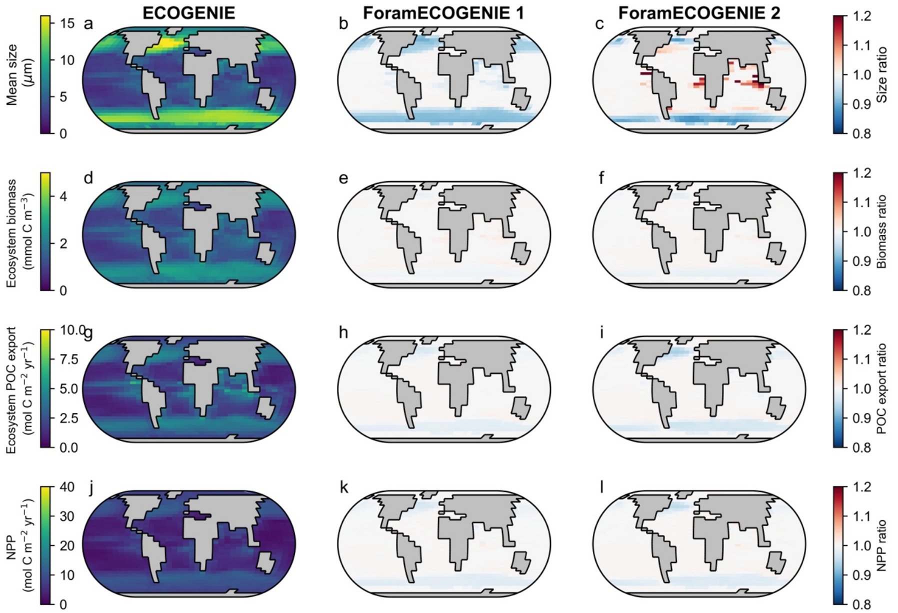

Figure 12. Tuned ForamEcoGENIE 2 (third column, with four foraminifer groups) comparison with ECOGENIE (first column) and ForamEcoGENIE 1 (second column, with non-spinose non-symbiont foraminifer only) in terms of ecosystem mean size, ecosystem biomass, ecosystem POC export, and Net Primary Production (NPP). The first column displays absolute values, whilst the latter two are the ratio relative to the first column.

9 Model limitation

Our model implementation has limitation due to our current gap in understanding trait. One is the not explicit definition of spine and symbiosis. For example, with the definition in Mitra et al., (2016), the current modelling approach falls within constitutive (inherent or innate) mixotroph rather than foraminifer's specialist non-constitutive mixotroph. Such indirect photosymbiotic relationships in the model could miss the individual climate sensitivities of symbiont and host. Meanwhile, the implicit definition of spines and symbiosis cannot lead to a changeable spine and symbiosis effects with environmental changes. And this is because we lack such observational studies.

Some detailed trait interaction and variation are not included as well. The symbiotic spinose foraminifer can use their spines to place algal symbionts in the daytime (LeKieffre et al., 2018), which theoretically increases photosynthesis efficiency due to an increase in surface area relative to non-spinose species. And the unclear relationship between body size and spine and symbiosis forces the model the fix the foraminifer size at 190 µm and ignore the biomass of juvenile foraminifer. From this perspective, our foraminifer model belongs to a functional-type model rather than a strict trait-based model. However, we also note this study focuses on solving the gap of modelling past time and resemble the functional biogeography of planktic foraminifer.

In addition to model implementation, the spatial or temporal sparseness of plankton net and sediment trap data make model-data comparison difficult. The M-score cannot reflect the model-data difference properly as there are limited grid points after annually averaging and regridding. The parameterisation is therefore highly influenced. The sediment trap data are temporally more continuous, but we still lack a vertical profile in different locations as most POC flux studies (Henson et al., 2012). The current model parameterisation for export production is compared with vertically averaged values. Therefore, the foraminifera surface carbon export should be higher than the model predicts and agree with the high proportion in Scheibel (2002). The reason behind observed low biomass and high carbon export is unclear but likely caused by the underestimated sampling. Because plankton net is temporally low-resolution and cannot capture the peak production signal.

10 Ecosystem model implementation and complexity

The current coupled Earth system models are mostly NPZD (Nutrient-Plankton-Zooplankton-Detritus) based (Keller et al., 2012; Watanabe et al., 2011), or PFT (Plankton Functional Type) based (Moore et al., 2001; Aumont et al., 2015). While NPZD models focus on the biogeochemical fluxes and have ignored different size classes and types within phytoplankton and zooplankton models, PFT models have more explicit functional types (e.g., diatom, coccolithophore) and size classes (e.g., picoplankton, nanoplankton, microplankton). This usually helps achieve better model performance in region scale. For example, the inclusion of diatom-diazotroph assemblages allows model to predict peak production in oligotrophic areas (Tréguer et al., 2018). Trait-based models as another member like Darwin (Follows et al., 2007) and EcoGENIE (Ward et al., 2018), solve the plankton diversity based on allometric rule. Therefore, the plankton size spectrum can be more continuous and physiological parameters can be calculated based on individual size. This is theoretically more robust especially when the model is used to simulate past ecology or large-scale pattern. However, these models also classify species into various

Deleted: (Mitra et al., 2016)

Deleted: ¶
5 Model limitation¶
The limitations in our current trait understanding still influence our model definition and performance. For example, symbiotic spinose foraminifer can use their spines to place algal symbionts in the daytime (LeKieffre et al., 2018), which theoretically increases photosynthesis efficiency due to an increase in surface area relative to non-spinose species. In this model, we do not explicitly model the photosymbiotic relationships which could be sensitive to individual climate sensitivities of symbiont and host. Similarly, spinose foraminifera prefer large zooplankton prey over phytoplankton as their prey, while non-spinose species are often herbivorous (Anderson et al., 1979). Such specialised behaviour is not resolved in the model and might explain why the symbiont-barren spinose *G. bulloides* do not show opportunistic behaviour, i.e., appear earlier than other groups in the seasonal succession (Taylor et al., 2018; Schiebel et al., 2001).

Formatted: Font: Bold

Formatted: Font: Not Bold

Formatted: Font: Not Bold, (Asian) Chinese (China) functional types according to evolutionary similarities. This might be because we cannot distinguish the ocean diversity by size trait only. More functional traits beyond size like symbiosis (Suggett et al., 2017) and body extension (Ohman, 2019) also play an important role in influencing plankton feeding, metabolism and export efficiency.

There is also a debate on whether higher ecosystem complexity is needed (See introduction in Quéré et al., 2005) because more parameters introduce more freedom, longer run time and the ocean physics influence biogeochemistry more than ecology. However, recent studies suggested the important role of biodiversity in the ocean biological pumps (Tréguer et al., 2018). The presence of functional group like diazotroph can even diverge the response trend to global warming (Bopp et al., 2022). Therefore, relative to the simple food web structure in current generation of models, ecosystem implementation is very likely the source of uncertainties for modelled ocean carbon storage in the future (Wilson et al., 2022). In addition, the recent model advances already included more supports to ecosystem complexities such as more functional types, variable stoichiometry, and nutrient co-limitations (Séférian et al., 2020). To our study, the significance of more functional traits also enables us to track the foraminifer functional diversity change and provide the likelihood of explicitly linking foraminifer ecology to carbonate pump in the future.

11 Summary

In this study, we extend the trait-based planktic foraminifer model, ForamEcoGENIE, to include symbiosis and spine traits and resolve all main foraminifer functional groups. Using Latin Hypercube Sampling, we generated 1,200 parameter samples and compared these with three global observational sources: core-top, plankton tow, sediment trap. We assessed the model performance of biogeographic distributions, the carbon biomass and foraminifer-derived carbon export. Our global sensitivity analysis shows the symbiosis trait and the palatability protection of spine and test strongly influence model performance. Our best set of model parameters successfully reproduces the modern biogeographical distribution of the main four foraminifera ecogroups and produces a global annual mean biomass (0.001 to 0.010 mmol C m^{-3}) and foraminifer-derived organic carbon export (0.002-0.031 mmol C m^{-2} d^{-1}) similar to observations. The two symbiont-barren groups account for 85% of standing stocks and foraminifer-derived carbon export, while the two symbiotic group contribute the remaining 15%. The model accurately reproduces peak time of seasonal time-series observations of foraminiferal biomass and organic carbon flux but performs poorly in seasonal amplitudes, particularly in upwelling regions. These results provide confidence in the model's ability to explore foraminifer ecology and diversity in the geological record and to interpret and question the foraminifer microfossil records, for example of the last glacial maximum, as well as helping to solve riddles about their ecology in the past. The trait-based framework of cGENIE ecosystem also provides potential to extend the model by presenting more traits such as life history and differential calcification rates across groups.

Code and data availability

Formatted: (Asian) Chinese (China), (Other) English (US)

Deleted: ¶
¶
¶

Formatted: (Asian) Chinese (China), (Other) English (US)

Deleted: 6

Deleted: Despite overestimating the overall biomass, o

Deleted:

Deleted: of 365.3 TgC yr^{-1}

Deleted: 64

Deleted: 36

Deleted: in large parts of the ocean

Deleted: in

Deleted: , probably due to the low model resolution

Deleted: The model suggests a foraminifera calcite export rate of 1.1 Gt yr^{-1}, equivalent to 19% of the global marine calcium carbonate budget. The value agrees with the lower end of modern estimates.

The source codes and data are archived in https:doi.org/10.5281/zenodo.6808760. Experiment configuration and observational dataset can be found in genie-userconfig/MS/yingetal.GMD.2022. More general manual for cGENIE model can be found in https://github.com/derpycode/muffindoc.

Deleted: https:10.5281/zenodo.6808761

Author contribution

RY, FMM, JDW, DNS designed the study. RY, FMM, JDW developed the model code. RY performed the experiments, data collection and visualisation. All authors wrote and edited the original draft.

Competing interests

The authors declare that they have no conflict of interest.

Acknowledgements

We acknowledge funding from Royal Society Wolfson Research Merit Award (DNS), NERC (NE/P019439/1 for DNS and JDW), NE/N011708/1 (FMM), TMS Angelina Messina Grant (RY), China Scholarship Council (RY, No. 202006380070), and AXA Research Fund Postdoctoral Fellowship (JDW). We would like to thank Maria Grigoratou for her insights on the model development.

References

Adloff, M., Ridgwell, A., Monteiro, F. M., Parkinson, I. J., Dickson, A. J., Pogge von Strandmann, P. A. E., Fantle, M. S., and Greene, S. E.: Inclusion of a suite of weathering tracers in the cGENIE Earth system model – muffin release v.0.9.23, Geosci. Model Dev., 14, 4187–4223, https://doi.org/10.5194/gmd-14-4187-2021, 2021.

Andersen, K. H., Berge, T., Gonçalves, R. J., Hartvig, M., Heuschele, J., Hylander, S., Jacobsen, N. S., Lindemann, C., Martens, E. A., Neuheimer, A. B., Olsson, K., Palacz, A., Prowe, A. E. F., Sainmont, J., Traving, S. J., Visser, A. W., Wadhwa, N., and Kiørboe, T.: Characteristic Sizes of Life in the Oceans, from Bacteria to Whales, Annual Review of Marine Science, 8, 217–241, https://doi.org/10/f3pdzr, 2016.

Anderson, O. R. and Bé, A. W. H.: The ultrastructure of a planktonic foraminifer, Globigerinoides sacculifer (Brady), and its symbiotic dinoflagellates, Journal of Foraminiferal Research, 6, 1–21, https://doi.org/10.2113/gsjfr.6.1.1, 1976.

Anderson, O. R., Spindler, M., Bé, A. W. H., and Hemleben, Ch.: Trophic activity of planktonic foraminifera, J. Mar. Biol. Ass., 59, 791–799, https://doi.org/10.1017/S002531540004577X, 1979.

Anon: Evaluation of a CMIP5 derived dynamical global wind wave climate model ensemble, Ocean Modelling, 103, 190–203, https://doi.org/10.1016/j.ocemod.2015.10.009, 2016.

Aumont, O., Ethé, C., Tagliabue, A., Bopp, L., and Gehlen, M.: PISCES-v2: an ocean biogeochemical model for carbon and ecosystem studies, Geoscientific Model Development, 8, 2465–2513, https://doi.org/10.5194/gmd-8-2465-2015, 2015.

Bé, A. W. H., Spero, H. J., and Anderson, O. R.: Effects of symbiont elimination and reinfection on the life processes of the planktonic foraminifer Globigerinoides sacculifer, Mar. Biol., 70, 73–86, https://doi.org/10.1007/BF00397298, 1982.

Bec, Bé., Collos, Y., Vaquer, A., Mouillot, D., and Souchu, P.: Growth rate peaks at intermediate cell size in marine photosynthetic picoeukaryotes, Limnol. Oceanogr., 53, 863–867, https://doi.org/10.4319/lo.2008.53.2.0863, 2008.

Bopp, L., Aumont, O., Kwiatkowski, L., Clerc, C., Dupont, L., Ethé, C., Gorgues, T., Séférian, R., and Tagliabue, A.: Diazotrophy as a key driver of the response of marine net primary productivity to climate change, Biogeosciences, 19, 4267–4285, https://doi.org/10.5194/bg-19-4267-2022, 2022.

Brovkin, V., Brücher, T., Kleinen, T., Zaehle, S., Joos, F., Roth, R., Spahni, R., Schmitt, J., Fischer, H., Leuenberger, M., Stone, E. J., Ridgwell, A., Chappellaz, J., Kehrwald, N., Barbante, C., Blunier, T., and Dahl Jensen, D.: Comparative carbon cycle dynamics of the present and last interglacial, Quaternary Science Reviews, 137, 15–32, https://doi.org/10.1016/j.quascirev.2016.01.028, 2016.

Brown, J. H., Gillooly, J. F., Allen, A. P., Savage, V. M., and West, G. B.: Toward a Metabolic Theory of Ecology, Ecology, 1771–1789, https://doi.org/10.1890/03-9000@10.1002/(ISSN)1939-9170.MacArthurAward, 2004.

Buckley, L. B., Urban, M. C., Angilletta, M. J., Crozier, L. G., Rissler, L. J., and Sears, M. W.: Can mechanism inform species' distribution models?, Ecology Letters, 13, 1041–1054, https://doi.org/10.1111/j.1461-0248.2010.01479.x, 2010.

Buitenhuis, E. T., Vogt, M., Moriarty, R., Bednaršek, N., Doney, S. C., Leblanc, K., Le Quéré, C., Luo, Y.-W., O'Brien, C., O'Brien, T., Peloquin, J., Schiebel, R., and Swan, C.: MAREDAT: towards a world atlas of MARine Ecosystem DATa, Earth System Science Data, 5, 227–239, https://doi.org/10.5194/essd-5-227-2013, 2013.

Buitenhuis, E. T., Quéré, C. L., Bednaršek, N., and Schiebel, R.: Large Contribution of Pteropods to Shallow CaCO3 Export, Global Biogeochemical Cycles, 33, 458–468, https://doi.org/10/gjpnzt, 2019.

Cao, L., Eby, M., Ridgwell, A., Caldeira, K., Archer, D., Ishida, A., Joos, F., Matsumoto, K., Mikolajewicz, U., Mouchet, A., Orr, J. C., Plattner, G.-K., Schlitzer, R., Tokos, K., Totterdell, I., Tschumi, T., Yamanaka, Y., and Yool, A.: The role of ocean transport in the uptake of anthropogenic CO2, Biogeosciences, 6, 375–390, https://doi.org/10/fp96kf, 2009.

Castellani, M., Våge, S., Strand, E., Thingstad, T. F., and Giske, J.: The Scaled Subspaces Method: A new trait-based approach to model communities of populations with largely inhomogeneous density, Ecological Modelling, 251, 173–186, https://doi.org/10.1016/j.ecolmodel.2012.12.006, 2013.

Daniels, C. J., Poulton, A. J., Balch, W. M., Marañón, E., Adey, T., Bowler, B. C., Cermeño, P., Charalampopoulou, A., Crawford, D. W., Drapeau, D., Feng, Y., Fernández, A., Fernández, E., Fragoso, G. M., González, N., Graziano, L. M., Heslop, R., Holligan, P. M., Hopkins, J., Huete-Ortega, M., Hutchins, D. A., Lam, P. J., Lipsen, M. S., López-Sandoval, D. C., Loucaides, S., Marchetti, A., Mayers, K. M. J., Rees, A. P., Sobrino, C., Tynan, E., and Tyrrell, T.: A global compilation of coccolithophore calcification rates, Earth Syst. Sci. Data, 10, 1859–1876, https://doi.org/10.5194/essd-10-1859-2018, 2018.

Droop, M. R.: Vitamin B12 and Marine Ecology. IV. The Kinetics of Uptake, Growth and Inhibition in Monochrysis Lutheri, J. Mar. Biol. Ass., 48, 689–733, https://doi.org/10.1017/S0025315400019238, 1968.

Edwards, K. F., Thomas, M. K., Klausmeier, C. A., and Litchman, E.: Allometric scaling and taxonomic variation in nutrient utilization traits and maximum growth rate of phytoplankton, Limnol. Oceanogr., 57, 554–566, https://doi.org/10.4319/lo.2012.57.2.0554, 2012.

Edwards, N. R. and Marsh, R.: Uncertainties due to transport-parameter sensitivity in an efficient 3-D ocean-climate model, Clim Dyn, 24, 415–433, https://doi.org/10/fcvq9k, 2005.

Ezard, T. H. G., Aze, T., Pearson, P. N., and Purvis, A.: Interplay Between Changing Climate and Species’ Ecology Drives Macroevolutionary Dynamics, Science, 332, 349–351, https://doi.org/10/bd77gm, 2011.

Fiksen, Ø., Follows, M. J., and Aksnes, D. L.: Trait-based models of nutrient uptake in microbes extend the Michaelis-Menten framework, Limnol. Oceanogr., 58, 193–202, https://doi.org/10.4319/lo.2013.58.1.0193, 2013.

Fisher, R. A., Corbet, A. S., and Williams, C. B.: The Relation Between the Number of Species and the Number of Individuals in a Random Sample of an Animal Population, Journal of Animal Ecology, 12, 42–58, https://doi.org/10.2307/1411, 1943.

Flynn, K. J.: The importance of the form of the quota curve and control of non-limiting nutrient transport in phytoplankton models, Journal of Plankton Research, 30, 423–438, https://doi.org/10.1093/plankt/fbn007, 2008.

Follows, M. J., Dutkiewicz, S., Grant, S., and Chisholm, S. W.: Emergent Biogeography of Microbial Communities in a Model Ocean, Science, 315, 1843–1846, https://doi.org/10/bf6j95, 2007.

Fraile, I., Schulz, M., Mulitza, S., and Kucera, M.: Predicting the global distribution of planktonic foraminifera using a dynamic ecosystem model, Biogeosciences, 5, 891–911, https://doi.org/10/dkjgd3, 2008.

Fraile, I., Schulz, M., Mulitza, S., Merkel, U., Prange, M., and Paul, A.: Modeling the seasonal distribution of planktonic foraminifera during the Last Glacial Maximum, Paleoceanography, 24, https://doi.org/10/dh2z9t, 2009.

Gaskell, D. E., Ohman, M. D., and Hull, P. M.: Zooglider-Based Measurements of Planktonic Foraminifera in the California Current System, Journal of Foraminiferal Research, 49, 390–404, https://doi.org/10.2113/gsjfr.49.4.390, 2019.

Geider, R. J., Maclntyre, H. L., and Kana, T. M.: A dynamic regulatory model of phytoplanktonic acclimation to light, nutrients, and temperature, Limnol. Oceanogr., 43, 679–694, https://doi.org/10.4319/lo.1998.43.4.0679, 1998.

Gregoire, L. J., Valdes, P. J., Payne, A. J., and Kahana, R.: Optimal tuning of a GCM using modern and glacial constraints, Clim Dyn, 37, 705–719, https://doi.org/10.1007/s00382-010-0934-8, 2011.

Grigoratou, M.: A trait-based approach to planktonic foraminifera ecology and biogeography, University of Bristol, 2019.

Grigoratou, M., Monteiro, F. M., Schmidt, D. N., Wilson, J. D., Ward, B. A., and Ridgwell, A.: A trait-based modelling approach to planktonic foraminifera ecology, Biogeosciences, 16, 1469–1492, https://doi.org/10/gj349g, 2019.

Grigoratou, M., Monteiro, F. M., Wilson, J. D., Ridgwell, A., and Schmidt, D. N.: Exploring the impact of climate change on the global distribution of non-spinose planktonic foraminifera using a trait-based ecosystem model, Glob Change Biol, gcb.15964, https://doi.org/10.1111/gcb.15964, 2021a.

Grigoratou, M., Monteiro, F. M., Ridgwell, A., and Schmidt, D. N.: Investigating the benefits and costs of spines and diet on planktonic foraminifera distribution with a trait-based ecosystem model, Marine Micropaleontology, 102004, https://doi.org/10/gkbn65, 2021b.

Hemleben, C., Spindler, M., and Erson, O. R.: Modern planktonic foraminifera, 363 pp., 1989.

Henehan, M. J., Ridgwell, A., Thomas, E., Zhang, S., Alegret, L., Schmidt, D. N., Rae, J. W. B., Witts, J. D., Landman, N. H., Greene, S. E., Huber, B. T., Super, J. R., Planavsky, N. J., and Hull, P. M.: Rapid ocean acidification and protracted Earth system recovery followed the end-Cretaceous Chicxulub impact, PNAS, 116, 22500–22504, https://doi.org/10/ggbnrm, 2019.

Henson, S. A., Sanders, R., and Madsen, E.: Global patterns in efficiency of particulate organic carbon export and transfer to the deep ocean, Global Biogeochemical Cycles, 26, https://doi.org/10.1029/2011GB004099, 2012.

Holling, C. S.: The Functional Response of Predators to Prey Density and its Role in Mimicry and Population Regulation, Mem. Entomol. Soc. Can., 97, 5–60, https://doi.org/10/fhjtms, 1965.

Hönisch, B., Ridgwell, A., Schmidt, D. N., Thomas, E., Gibbs, S. J., Sluijs, A., Zeebe, R., Kump, L., Martindale, R. C., Greene, S. E., Kiessling, W., Ries, J., Zachos, J. C., Royer, D. L., Barker, S., Marchitto, T. M., Moyer, R., Pelejero, C., Ziveri, P., Foster, G. L., and Williams, B.: The Geological Record of Ocean Acidification, Science, 335, 1058–1063, https://doi.org/10/gdj3zf, 2012.

Jarman, A. M.: Hierarchical cluster analysis: Comparison of single linkage, complete linkage, average linkage and centroid linkage method, Georgia Southern University, 2020.

Jonkers, L. and Kučera, M.: Global analysis of seasonality in the shell flux of extant planktonic Foraminifera, Biogeosciences, 12, 2207–2226, https://doi.org/10.5194/bg-12-2207-2015, 2015.

Keller, D. P., Oschlies, A., and Eby, M.: A new marine ecosystem model for the University of Victoria Earth System Climate Model, Geoscientific Model Development, 5, 1195–1220, https://doi.org/10.5194/gmd-5-1195-2012, 2012.

Kiørboe, T., Visser, A., and Andersen, K. H.: A trait-based approach to ocean ecology, ICES Journal of Marine Science, 75, 1849–1863, https://doi.org/10.1093/icesjms/fsy090, 2018.

Kretschmer, K., Jonkers, L., Kucera, M., and Schulz, M.: Modeling seasonal and vertical habitats of planktonic foraminifera on a global scale, Biogeosciences, 15, 4405–4429, https://doi.org/10/gdx3bj, 2018.

LeKieffre, C., Spero, H. J., Russell, A. D., Fehrenbacher, J. S., Geslin, E., and Meibom, A.: Assimilation, translocation, and utilization of carbon between photosynthetic symbiotic dinoflagellates and their planktic foraminifera host, Mar Biol, 165, 104, https://doi.org/10/gj35br, 2018.

Lombard, F., Labeyrie, L., Michel, E., Bopp, L., Cortijo, E., Retailleau, S., Howa, H., and Jorissen, F.: Modelling planktic foraminifer growth and distribution using an ecophysiological multi-species approach, Biogeosciences, 8, 853–873, https://doi.org/10.5194/bg-8-853-2011, 2011.

Marsh, R., Müller, S. A., Yool, A., and Edwards, N. R.: Incorporation of the C-GOLDSTEIN efficient climate model into the GENIE framework: “eb_go_gs” configurations of GENIE, Geoscientific Model Development, 4, 957–992, https://doi.org/10.5194/gmd-4-957-2011, 2011.

Meyer, K. M., Kump, L. R., and Ridgwell, A.: Biogeochemical controls on photic-zone euxinia during the end-Permian mass extinction, Geol, 36, 747, https://doi.org/10.1130/G24618A.1, 2008.

Mitra, A., Flynn, K. J., Tillmann, U., Raven, J. A., Caron, D., Stoecker, D. K., Not, F., Hansen, P. J., Hallegraeff, G., Sanders, R., Wilken, S., McManus, G., Johnson, M., Pitta, P., Våge, S., Berge, T., Calbet, A., Thingstad, F., Jeong, H. J., Burkholder, J., Glibert, P. M., Granéli, E., and Lundgren, V.: Defining Planktonic Protist Functional Groups on Mechanisms for Energy and Nutrient Acquisition: Incorporation of Diverse Mixotrophic Strategies, Protist, 167, 106–120, https://doi.org/10/f3p5h2, 2016.

Monteiro, F. M., Follows, M. J., and Dutkiewicz, S.: Distribution of diverse nitrogen fixers in the global ocean, Global Biogeochem. Cycles, 24, n/a-n/a, https://doi.org/10/ctkc4h, 2010.

Moore, J. K., Doney, S. C., Kleypas, J. A., Glover, D. M., and Fung, I. Y.: An intermediate complexity marine ecosystem model for the global domain, Deep Sea Research Part II: Topical Studies in Oceanography, 49, 403–462, https://doi.org/10/bp99zn, 2001.

Ohman, M. D.: A sea of tentacles: optically discernible traits resolved from planktonic organisms in situ, ICES Journal of Marine Science, 76, 1959–1972, https://doi.org/10.1093/icesjms/fsz184, 2019.

Ortiz, J. D., Mix, A. C., and Collier, R. W.: Environmental control of living symbiotic and asymbiotic foraminifera of the California Current, Paleoceanography, 10, 987–1009, https://doi.org/10/ft8jc7, 1995.

Pianosi, F. and Wagener, T.: A simple and efficient method for global sensitivity analysis based on cumulative distribution functions, Environmental Modelling & Software, 67, 1–11, https://doi.org/10/f677qs, 2015.

Quéré, C. L., Harrison, S. P., Prentice, I. C., Buitenhuis, E. T., Aumont, O., Bopp, L., Claustre, H., Cunha, L. C. D., Geider, R., Giraud, X., Klaas, C., Kohfeld, K. E., Legendre, L., Manizza, M., Platt, T., Rivkin, R. B., Sathyendranath, S., Uitz, J., Watson, A. J., and Wolf-Gladrow, D.: Ecosystem dynamics based on plankton functional types for global ocean biogeochemistry models, Global Change Biology, 11, 2016–2040, https://doi.org/10/cm9nzc, 2005.

R Core Team: R: A Language and Environment for Statistical Computing, R Foundation for Statistical Computing, Vienna, Austria, 2021.

Rae, J. W. B., Gray, W. R., Wills, R. C. J., Eisenman, I., Fitzhugh, B., Fotheringham, M., Littley, E. F. M., Rafter, P. A., Rees-Owen, R., Ridgwell, A., Taylor, B., and Burke, A.: Overturning circulation, nutrient limitation, and warming in the Glacial North Pacific, Science Advances, 6, eabd1654, https://doi.org/10/ghrj7m, 2020.

Renaud, S. and Schmidt, D. N.: Habitat tracking as a response of the planktic foraminifer Globorotalia truncatulinoides to environmental fluctuations during the last 140 kyr, Marine Micropaleontology, 49, 97–122, https://doi.org/10/bgp3cz, 2003.

Ridgwell, A. and Hargreaves, J. C.: Regulation of atmospheric CO_2 by deep-sea sediments in an Earth system model: REGULATION OF CO_2 BY DEEP-SEA SEDIMENTS, Global Biogeochem. Cycles, 21, n/a-n/a, https://doi.org/10.1029/2006GB002764, 2007.

Ridgwell, A. and Schmidt, D. N.: Past constraints on the vulnerability of marine calcifiers to massive carbon dioxide release, Nature Geosci, 3, 196–200, https://doi.org/10.1038/ngeo755, 2010.

Ridgwell, A., Hargreaves, J. C., Edwards, N. R., Annan, J. D., Lenton, T. M., Marsh, R., Yool, A., and Watson, A.: Marine geochemical data assimilation in an efficient Earth System Model of global biogeochemical cycling, Biogeosciences, 4, 87–104, https://doi.org/10/dcq62d, 2007.

Roy, T., Lombard, F., Bopp, L., and Gehlen, M.: Projected impacts of climate change and ocean acidification on the global biogeography of planktonic Foraminifera, Biogeosciences, 12, 2873–2889, https://doi.org/10/f7gcgw, 2015.

Salter, I., Schiebel, R., Ziveri, P., Movellan, A., Lampitt, R., and Wolff, G. A.: Carbonate counter pump stimulated by natural iron fertilization in the Polar Frontal Zone, Nature Geoscience, 7, 885–889, https://doi.org/10.1038/ngeo2285, 2014.

Sarrazin, F., Pianosi, F., and Wagener, T.: Global Sensitivity Analysis of environmental models: Convergence and validation, Environmental Modelling & Software, 79, 135–152, https://doi.org/10/f8n8kp, 2016.

Schiebel, R.: Planktic foraminiferal sedimentation and the marine calcite budget, Global Biogeochemical Cycles, 16, 3-1-3–21, https://doi.org/10/bdxfhs, 2002.

Schiebel, R. and Hemleben, C.: Planktic Foraminifers in the Modern Ocean, Springer Berlin Heidelberg, Berlin, Heidelberg, https://doi.org/10.1007/978-3-662-50297-6, 2017.

Schiebel, R. and Movellan, A.: First-order estimate of the planktic foraminifer biomass in the modern ocean, Earth System Science Data, 4, 75–89, https://doi.org/10.5194/essd-4-75-2012, 2012.

Schmidt, D. N., Thierstein, H. R., Bollmann, J., and Schiebel, R.: Abiotic Forcing of Plankton Evolution in the Cenozoic, Science, 303, 207–210, https://doi.org/10/b37mvn, 2004.

van Sebille, E., Scussolini, P., Durgadoo, J. V., Peeters, F. J. C., Biastoch, A., Weijer, W., Turney, C., Paris, C. B., and Zahn, R.: Ocean currents generate large footprints in marine palaeoclimate proxies, Nat Commun, 6, 6521, https://doi.org/10/f67xqv, 2015.

Séférian, R., Berthet, S., Yool, A., Palmiéri, J., Bopp, L., Tagliabue, A., Kwiatkowski, L., Aumont, O., Christian, J., Dunne, J., Gehlen, M., Ilyina, T., John, J. G., Li, H., Long, M. C., Luo, J. Y., Nakano, H., Romanou, A., Schwinger, J., Stock, C., Santana-Falcón, Y., Takano, Y., Tjiputra, J., Tsujino, H., Watanabe, M., Wu, T., Wu, F., and Yamamoto, A.: Tracking Improvement in Simulated Marine Biogeochemistry Between CMIP5 and CMIP6, Curr Clim Change Rep, 6, 95–119, https://doi.org/10.1007/s40641-020-00160-0, 2020.

Siccha, M. and Kucera, M.: ForCenS, a curated database of planktonic foraminifera census counts in marine surface sediment samples, Sci Data, 4, 170109, https://doi.org/10.1038/sdata.2017.109, 2017.

Silge, J., Chow, F., Kuhn, M., and Wickham, H.: rsample: General resampling infrastructure, 2021.

Spero, H. J. and Parker, S. L.: Photosynthesis in the symbiotic planktonic foraminifer Orbulina universa, and its potential contribution to oceanic primary productivity, Journal of Foraminiferal Research, 15, 273–281, https://doi.org/10/c2rt2q, 1985.

Suggett, D. J., Warner, M. E., and Leggat, W.: Symbiotic Dinoflagellate Functional Diversity Mediates Coral Survival under Ecological Crisis, Trends in Ecology & Evolution, 32, 735–745, https://doi.org/10.1016/j.tree.2017.07.013, 2017.

Sunagawa, S., Acinas, S. G., Bork, P., Bowler, C., Eveillard, D., Gorsky, G., Guidi, L., Iudicone, D., Karsenti, E., Lombard, F., Ogata, H., Pesant, S., Sullivan, M. B., Wincker, P., and de Vargas, C.: Tara Oceans: towards global ocean ecosystems biology, Nat Rev Microbiol, 18, 428–445, https://doi.org/10.1038/s41579-020-0364-5, 2020.

Takagi, H., Kimoto, K., Fujiki, T., Saito, H., Schmidt, C., Kucera, M., and Moriya, K.: Characterizing photosymbiosis in modern planktonic foraminifera, Biogeosciences, 16, 3377–3396, https://doi.org/10/gj35bq, 2019.

Takahashi, K. and Be, A. W. H.: Planktonic foraminifera: factors controlling sinking speeds, Deep Sea Research Part A. Oceanographic Research Papers, 31, 1477–1500, https://doi.org/10.1016/0198-0149(84)90083-9, 1984.

Tierney, J. E., Poulsen, C. J., Montañez, I. P., Bhattacharya, T., Feng, R., Ford, H. L., Hönisch, B., Inglis, G. N., Petersen, S. V., Sagoo, N., Tabor, C. R., Thirumalai, K., Zhu, J., Burls, N. J., Foster, G. L., Goddéris, Y., Huber, B. T., Ivany, L. C., Kirtland Turner, S., Lunt, D. J., McElwain, J. C., Mills, B. J. W., Otto-Bliesner, B. L., Ridgwell, A., and Zhang, Y. G.: Past climates inform our future, Science, 370, eaay3701, https://doi.org/10/gh6c3g, 2020.

Todd, C. L., Schmidt, D. N., Robinson, M. M., and Schepper, S. D.: Planktic Foraminiferal Test Size and Weight Response to the Late Pliocene Environment, Paleoceanography and Paleoclimatology, 35, e2019PA003738, https://doi.org/10/ghrd4r, 2020.

Tréguer, P., Bowler, C., Moriceau, B., Dutkiewicz, S., Gehlen, M., Aumont, O., Bittner, L., Dugdale, R., Finkel, Z., Iudicone, D., Jahn, O., Guidi, L., Lasbleiz, M., Leblanc, K., Levy, M., and Pondaven, P.: Influence of diatom diversity on the ocean biological carbon pump, Nature Geoscience, 11, 27–37, https://doi.org/10/gcxznd, 2018.

Uhle, M. E., Macko, S. A., Spero, H. J., Lea, D. W., Ruddiman, W. F., and Engel, M. H.: The fate of nitrogen in the Orbulina universa foraminifera-symbiont system determined by nitrogen isotope analyses of shell-bound organic matter, Limnol. Oceanogr., 44, 1968–1977, https://doi.org/10/ffgtfw, 1999.

Våge, S., Castellani, M., Giske, J., and Thingstad, T. F.: Successful strategies in size structured mixotrophic food webs, Aquat Ecol, 47, 329–347, https://doi.org/10.1007/s10452-013-9447-y, 2013.

van de Velde, S. J., Hülse, D., Reinhard, C. T., and Ridgwell, A.: Iron and sulfur cycling in the cGENIE.muffin Earth system model (v0.9.21), Geosci. Model Dev., 14, 2713–2745, https://doi.org/10.5194/gmd-14-2713-2021, 2021.

Ward, B. A. and Follows, M. J.: Marine mixotrophy increases trophic transfer efficiency, mean organism size, and vertical carbon flux, Proc Natl Acad Sci USA, 113, 2958–2963, https://doi.org/10/ggnmm5, 2016.

Ward, B. A., Wilson, J. D., Death, R. M., Monteiro, F. M., Yool, A., and Ridgwell, A.: EcoGEnIE 1.0: plankton ecology in the cGEnIE Earth system model, Geosci. Model Dev., 11, 4241–4267, https://doi.org/10/gfjrbk, 2018.

Watanabe, S., Hajima, T., Sudo, K., Nagashima, T., Takemura, T., Okajima, H., Nozawa, T., Kawase, H., Abe, M., Yokohata, T., Ise, T., Sato, H., Kato, E., Takata, K., Emori, S., and Kawamiya, M.: MIROC-ESM 2010: model description and basic results of CMIP5-20c3m experiments, Geoscientific Model Development, 4, 845–872, https://doi.org/10.5194/gmd-4-845-2011, 2011.

Waterson, A. M., Edgar, K. M., Schmidt, D. N., and Valdes, P. J.: Quantifying the stability of planktic foraminiferal physical niches between the Holocene and Last Glacial Maximum: Niche Stability of Planktic Foraminifera, Paleoceanography, 32, 74–89, https://doi.org/10/f9vbtb, 2017.

Watterson, I. G.: Non-Dimensional Measures of Climate Model Performance, International Journal of Climatology, 16, 379–391, https://doi.org/10.1002/(SICI)1097-0088(199604)16:4<379::AID-JOC18>3.0.CO;2-U, 1996.

Watterson, I. G., Bathols, J., and Heady, C.: What Influences the Skill of Climate Models over the Continents?, Bulletin of the American Meteorological Society, 95, 689–700, https://doi.org/10.1175/BAMS-D-12-00136.1, 2014.

West, G. B., Brown, J. H., and Enquist, B. J.: A General Model for the Origin of Allometric Scaling Laws in Biology, Science, 276, 122–126, https://doi.org/10.1126/science.276.5309.122, 1997.

Wilson, J. D., Andrews, O., Katavouta, A., de Melo Viríssimo, F., Death, R. M., Adloff, M., Baker, C. A., Blackledge, B., Goldsworth, F. W., Kennedy-Asser, A. T., Liu, Q., Sieradzan, K. R., Vosper, E., and Ying, R.: The biological carbon pump in CMIP6 models: 21st century trends and uncertainties, Proc. Natl. Acad. Sci. U.S.A., 119, e2204369119, https://doi.org/10.1073/pnas.2204369119, 2022.

Zakharova, L., Meyer, K. M., and Seifan, M.: Trait-based modelling in ecology: A review of two decades of research, Ecological Modelling, 407, 108703, https://doi.org/10.1016/j.ecolmodel.2019.05.008, 2019.

Žarić, S., Schulz, M., and Mulitza, S.: Global prediction of planktic foraminiferal fluxes from hydrographic and productivity data, Biogeosciences, 3, 187–207, https://doi.org/10/ddgc7j, 2006.

Page 4: [1] Deleted Rui Ying 23/10/2022 12:45:00

Page 4: [2] Deleted Rui Ying 07/11/2022 22:07:00

Page 11: [3] Deleted Rui Ying 08/11/2022 14:28:00

Page 11: [4] Deleted Rui Ying 08/11/2022 14:33:00

Page 11: [5] Deleted Rui Ying 08/11/2022 13:20:00

Page 12: [6] Deleted Rui Ying 09/11/2022 14:47:00

Page 16: [7] Deleted Rui Ying 28/10/2022 12:14:00

Page 16: [8] Deleted Rui Ying 09/11/2022 13:49:00

Page 16: [8] Deleted Rui Ying 09/11/2022 13:49:00

Page 16: [9] Deleted Rui Ying 04/11/2022 00:42:00

Page 16: [10] Deleted Rui Ying 04/11/2022 19:04:00

Page 16: [10] Deleted Rui Ying 04/11/2022 19:04:00

Page 16: [10] Deleted Rui Ying 04/11/2022 19:04:00

Page 18: [11] Deleted Rui Ying 04/11/2022 11:09:00

Page 18: [11] Deleted Rui Ying 04/11/2022 11:09:00

Page 18: [12] Deleted Rui Ying 08/11/2022 13:29:00

Page 18: [12] Deleted Rui Ying 08/11/2022 13:29:00

Page 18: [13] Formatted Rui Ying 02/11/2022 19:24:00

Not Superscript/ Subscript

Page 18: [13] Formatted Rui Ying 02/11/2022 19:24:00

Not Superscript/ Subscript

Page 20: [14] Deleted Rui Ying 02/11/2022 14:20:00